AEDC-TSR-89-V25

AD-A217 672

INVESTIGATION OF THE DEVELOPMENT

OF LAMINAR BOUNDARY-LAYER INSTABILITIES ALONG

A COOLED-WALL HOLLOW CYLINDER

AT MACH NUMBER 8

J.C. Donaldson and D.W. Sinclair
Calspan Corporation/AEDC Operations

January 1990

Final Report for August 3-14, 1989

DTIC
ELECTE
JAN 25 1990
S E D

ARNOLD ENGINEERING DEVELOPMENT CENTER
ARNOLD AIR FORCE BASE, TENNESSEE
AIR FORCE SYSTEMS COMMAND
UNITED STATES AIR FORCE

90 01 24 0 53

DESTRUCTION NOTICE

For classified documents, follow the procedures in DoD 5200.22-M, Industrial Security Manual, Section II-19 or DoD 5200.1-R, Information Security Program Regulation, Chapter IX. For unclassified, limited documents, destroy by any method that will prevent disclosure or reconstruction of the document.

APPROVAL STATEMENT

This report has been reviewed and approved.

NORMAN H. PATNODE, Capt, USAF
Reentry Systems Division
Dir of Aerospace Flt Dyn Test
Deputy for Operations

Approved for publication:

FOR THE COMMANDER

MICHAEL L. DELORENZO, Maj, USAF
Dep Dir, Aerospace Flt Dyn Test
Deputy for Operations

REPORT DOCUMENTATION PAGE

Public reporting burden for this collection of information is estimated to average 1 hour per response, including the time for reviewing instructions, searching existing data sources, gathering and maintaining the data needed, and completing and reviewing the collection of information. Send comments regarding this burden estimate or any other aspect of this collection of information, including suggestions for reducing this burden, to Washington Headquarters Services, Directorate for Information Operations and Reports, 1215 Jefferson Davis Highway, Suite 1204, Arlington, VA 22202-4302, and to the Office of Management and Budget, Paperwork Reduction Project (0704-0188), Washington, DC 20503.

1. AGENCY USE ONLY (Leave blank)	2. REPORT DATE	3. REPORT TYPE AND DATES COVERED
	January 1990	Final Report for 3-14 August 89

4. TITLE AND SUBTITLE	5. FUNDING NUMBERS
Investigation of the Development of Laminar Boundary-Layer Instabilities Along a Cooled-Wall Hollow Cylinder at Mach Number 8	PE JPF170 & 65807F

6. AUTHOR(S)

Donaldson, J. C. and Sinclair, D. W., Calspan Corporation/AEDC Operations

7. PERFORMING ORGANIZATION NAME(S) AND ADDRESS(ES)	8. PERFORMING ORGANIZATION REPORT NUMBER
Arnold Engineering Development Center/DOF Air Force Systems Command Arnold Air Force Base, TN 37389-5000	AEDC-TSR-89-V25

9. SPONSORING/MONITORING AGENCY NAMES(S) AND ADDRESS(ES)	10. SPONSORING/MONITORING AGENCY REPORT NUMBER
WRDC/FIMG Wright-Patterson AFB, OH 45433	

11. SUPPLEMENTARY NOTES

Available in Defense Technical Information Center (DTIC).

12a. DISTRIBUTION/AVAILABILITY STATEMENT	12b. DISTRIBUTION CODE
Approved for public release; distribution is unlimited.	

13. ABSTRACT (Maximum 200 words)

Measurements of fluctuating-flow and mean-flow parameters were made in the boundary layer on a cooled-wall hollow cylinder model in an investigation of the stability of laminar boundary layers in hypersonic flow. The flow-fluctuation measurements were made using constant-current hot-wire anemometry techniques. Boundary-layer profiles and model surface conditions were measured to supplement the hot-wire data. Testing was done at Mach number 8 with free-stream unit Reynolds numbers of 1.0 and 1.5 million per foot. The test equipment, test techniques, and the data acquisition and reduction procedures are described. Analysis of the hot-wire anemometer data is beyond the scope of this report.

14. SUBJECT TERMS		15. NUMBER OF PAGES
hypersonic flow, wind tunnel flow cold-wall model	boundary-layer stability hot-wire anemometry hollow cylinder	46
		16. PRICE CODE

17. SECURITY CLASSIFICATION OF REPORT	18. SECURITY CLASSIFICATION OF THIS PAGE	19. SECURITY CLASSIFICATION OF ABSTRACT	20. LIMITATION OF ABSTRACT
UNCLASSIFIED	UNCLASSIFIED	UNCLASSIFIED	SAME AS REPORT

COMPUTER GENERATED

CONTENTS

ILLUSTRATIONS

Figure

TABLES

SAMPLE DATA

NOMENCLATURE

ALPHA	Angle of attack, deg
$C(t_n)$	Coefficient in equation for calculating QDOT, $Btu/ft^2-sec^{1/2}-°R$
CONFIG	Model configuration designation
CURRENT	Hot-wire anemometer heating current, mAmp
DATA TYPE	Code indicating nature of data tabulated:
	"2" - Model surface pressure and temperature measurements
	"4" - Mean boundary-layer profile measurements using pitot pressure probe
	"9" - Hot-film anemometer probe measurements
DEL	Boundary-layer total thickness, in.
DEL*	Boundary-layer displacement thickness, in.
DEL**	Boundary-layer momentum thickness, in.
DEW	Tunnel stilling chamber dew point temperature, °F
DITTD	Enthalpy difference at boundary-layer thickness, DEL, ITTD-ITWL, Btu/lbm
DITTL	Local enthalpy difference, ITTL-ITWL, Btu/lbm
EBAR	Hot-wire anemometer mean voltage, mv
ERMS	Hot-wire anemometer output rms voltage, mv rms
FIL	Identification of data file used for plot
GAGE	Identification for coaxial thermocouple gage
H (TT), HT (TT)	Heat-transfer coefficient based on TT, QDOT/(TT-TW), $Btu/ft^2-sec-°R$
ITT	Enthalpy based on TT, Btu/lbm
ITTD	Enthalpy based on TTD, Btu/lbm
ITTL	Enthalpy based on TTL, Btu/lbm
ITW	Enthalpy based on TW, Btu/lbm
ITWL	Enthalpy based on TWL, Btu/lbm

2

LRE	Local unit Reynolds number, in.$^{-1}$
LRED	Unit Reynolds number at the boundary-layer thickness, DEL, in.$^{-1}$
LRET	Local "normal shock" unit Reynolds number (based on MUTTL), in.$^{-1}$
LRETD	"Normal shock" unit Reynolds number at boundary-layer thickness, DEL, (based on MUTTD), in.$^{-1}$
M, MACH	Free-stream Mach number
MD	Local Mach number at boundary-layer thickness, DEL
ME	Mach number at boundary-layer edge
ML	Local Mach number
MU	Dynamic viscosity based on T, lbf-sec/ft^2
MUTD	Dynamic viscosity based on TD, lbf-sec/ft^2
MUTL	Dynamic viscosity based on TL, lbf-sec/ft^2
MUTTD	Dynamic viscosity based on TTD, lbf-sec/ft^2
MUTTL	Dynamic viscosity based on TTL, lbf-sec/ft^2
P	Free-stream static pressure, psia
POINT	Data point number
PP	Pitot probe pressure, psia
PPD	Pitot pressure at boundary-layer thickness, DEL, psia
PPE	Pitot pressure at boundary-layer edge, psia
PT	Tunnel stilling chamber pressure, psia
PT2	Free-stream total pressure downstream of a normal shock wave, psia
PW	Model surface pressure, psia
PWL	Model wall static pressure used for boundary-layer survey calculations, psia
Q	Free-stream dynamic pressure, psia

QDOT	Heat-transfer rate, Btu/ft^2-sec
RE	Free-stream unit Reynolds number, in.$^{-1}$ or ft^{-1}
RE/FT	Free-stream unit Reynolds number, ft^{-1}
RHO	Free-stream density, lbm/ft^3
RHOD, RHD	Density at boundary-layer thickness, DEL, lbm/ft^3
RHOL, RHL	Local density, lbm/ft^3
RHOUD	(RHOD) * (UD), lbm/sec-ft^2
RN	Radius of model leading edge, in.
RUN	Data set identification number
ST(TT)	Stanton number based on stilling chamber temperature (TT),

$$ST(TT) = \frac{QDOT}{(RHO)\,(V)\,(ITT-ITW)}$$

T	Free-stream static temperature, °R, or °F
ΔT	Temperature difference, °F
TAP	Pressure orifice identification number
T/C	Identification number of model surface thermocouples
TD	Static temperature at boundary-layer thickness, DEL, °R
TDRK	Temperature of Druck probe transducer, °F
THETA	Peripheral angle on the model measured from ray on model top, positive clockwise when looking upstream, deg
TL	Local static temperature, °R
TT	Tunnel stilling chamber temperature, °R, or °F
TTD	Total temperature at boundary-layer thickness, DEL, °R
TTE	Total temperature at boundary-layer edge, °R
TTL	Local total temperature, °R
TW	Coaxial thermocouple gage surface temperature, °R

TW (t_j)	Coaxial thermocouple gage surface temperature at time point t_j, $j = 1$ to n, °R
TWL	Model wall temperature used for boundary-layer survey calculations, °R
TWTR	Water supply temperature, °R
t_j	Time point number j, $j = 1$ to n, sec
UD	Local velocity component parallel to model surface at boundary-layer thickness, DEL, ft/sec
UE	Local velocity component parallel to model surface at boundary-layer edge, ft/sec
UL	Local velocity component parallel to model surface, ft/sec
V	Free-stream velocity, ft/sec
X	Axial location measured from leading edge of model, in.
XC	Calculated X location of survey station, in.
XSTA	Nominal X location of survey station, in.
ZA	Anemometer probe height, distance to probe centerline along normal to model surface, in.
ZP	Pitot-pressure probe height, distance to probe centerline along normal to model surface, in.

5

1.0 INTRODUCTION

The work reported herein was performed by the Arnold Engineering Development Center (AEDC), Air Force Systems Command (AFSC), under Program Element Numbers JPF170 and 65807F, Control Numbers 1999 and 9T03, at the request of the Wright Research and Development Center (WRDC/FIMG), Wright-Patterson Air Force Base, Ohio 45433-6553, and the AEDC Directorate of Aerospace Flight Dynamics Test (AEDC/DOF). The WRDC project manager was Kenneth F. Stetson and the AEDC/DOF program manager was Capt. N. H. Patnode. The results were obtained by the Calspan Corporation/AEDC Operations, operating contractor for the Aerospace Flight Dynamics testing effort at the AEDC, AFSC, Arnold Air Force Base, Tennessee 37389-5000. The test was conducted in the AEDC Hypersonic Wind Tunnel (B) on August 3-14, 1989, under the AEDC Project Number C010VB (Calspan Project Number V--B-2R).

The objective of this test was to investigate the development of hypersonic laminar boundary-layer flow instabilities along a hollow cylinder model. The test was the eighth in a series of cooperative efforts between WRDC/FIMG ad AEDC/DOF. The first seven tests have investigated various aspects of boundary-layer stability on sharp and blunt cones. Representative documentation of the previous seven tests is given in Refs. 1-4. Selected results of the previous tests are presented in Refs. 5-9.

An existing water-cooled hollow cylinder model from the AEDC model inventory was used for the test. The principal measurements of this investigation were hot-wire anemometer probe data acquired above the top (zero) ray of the model. These data were supplemented by surveys of the model boundary layer using a pitot pressure probe. Model surface pressure, temperature, and heat-flux were also measured. Data were acquired at Mach number 8 for zero model angle of attack. In general the testing was done at free-stream unit Reynolds numbers of 1.0- and 1.5-million per foot. A limited amount of heat-transfer data was obtained at a unit Reynolds number of 2.0 million per foot.

Inquiries to obtain copies of the test data should be directed to AEDC/DOF, Arnold Air Force Base, Tennessee 37389-5000, or to WRDC/FIMG, Wright-Patterson Air Force Base, Ohio 45433-6553. A microfiche record has been retained at AEDC.

2.0 APPARATUS

2.1 TEST FACILITY

The AEDC Hypersonic Wind Tunnel B (Fig. 1) is a closed-circuit wind tunnel with a 50-in.-diameter test section. Two axisymmetric contoured nozzles are available to provide Mach numbers of 6 and 8, and the tunnel may be operated continuously over a range of pressure from 20 to 300 psia at Mach number 6, and 50 to 900 psia at Mach number 8,

with air supplied by the VKF main compressor plant. Stagnation temperatures sufficient to avoid air liquefaction in the test section (up to 1350°R) are obtained through the use of a natural gas fired combustion heater. The entire tunnel (throat, nozzle, test section, and diffuser) is cooled by integral, external water jackets. The tunnel is equipped with a model injection system, which allows removal of the model from the test section while the tunnel remains in operation. A description of the tunnel and airflow calibration information may be found in Ref. 10.

2.2 TEST ARTICLE

The test article used in this investigation (Fig. 2) was a hollow cylinder model with a length of 59.5 in., an O.D. of 10.0-in., and an I.D. of 8.1 in., out of AEDC model inventory. The cylinder was composed of two concentric shells of 0.2-in. wall thickness separated by stiffeners with provision for circulating cooling water in the space between the shells. The model had a removable leading edge section of 3.74-in. axial length with a sharp leading edge of 0.004-in. radius. The leading edge was beveled on the inside with an entry angle bevel of 15 deg. This section capped the upstream end of the coolant passage between the inner and outer shells of the cylinder. Cooling water was carried to the upstream end of the passage by eight tubes, evenly spaced circumferentially, where it was introduced just inside the leading edge section and allowed to diffuse to the downstream sealed end of the coolant passage. The water passage was full at all times during testing. A photograph of the test installation is shown in Fig. 3.

In order that air flow through the inner bore of the cylinder be unobstructed, it was necessary that the model support be attached to the outer surface of the model. The test article was mounted on the Tunnel B sector using a specially designed sting and a collar which attached over the aft 7.5 in. of the cylinder length (Fig. 2). The collar had an O.D. of 10.72 in. The leading edge of the collar was beveled to reduce the flow disturbance produced in the boundary layer by the joint. Surveys of the boundary layer were made 15 in. or more upstream of the leading edge of this collar. Cooling water was supplied to and drained from the cylinder through manifolds in the collar. Covered channels in the collar were provided to route the instrumentation tubes and leads from the cylinder to the sting.

The model was instrumented for the present test with 26 pressure orifices along four rays of the cylinder: eight orifices along the 15-deg ray and six orifices along each of the rays at 90, 180, and 270 deg. Coaxial thermocouple gages were installed at 27 locations along the 345-deg ray. The locations of the orifices and gages are listed in Table 1. Gages and the leads were encased in stainless steel tubing to seal them from the water flowing around them inside the coolant passage. Tubes from the pressure orifices and for the gage leads were sealed in the flange where they passed through the downstream end of the coolant passage.

7

2.3 FLOW-FIELD SURVEY MECHANISM

Surveys of the flow field were made using a retractable survey system (X-Z Survey Mechanism) designed and fabricated by the AEDC. This mechanism makes it possible to change survey probes while the tunnel remains in operation. The mechanism is housed in an air lock immediately above a port in the top of the Tunnel B test section. Access to the test section is through a 40-in.-long by 4-in.-wide opening which is sealed by a pneumatically operated door when the mechanism is retracted. Separate drive motors are provided to (1) insert the mechanism into the test section or retract it into the housing (Z drive), (2) position the mechanism at any desired axial station over a range of 35 in. (X drive), and (3) survey a flow field of approximately 10-in. depth (Z' drive). A pneumatically operated shield is provided to protect the probes during injection and retraction through the tunnel boundary layer, during changes in tunnel conditions, and at all times when the probes are not in use (Figs. 3 and 4a).

The probes required for flow-field survey measurements were rake-mounted on the X-Z mechanism (Fig. 4) at the foot of the Z' drive strut that was extended or retracted to accomplish the survey. The angle of the survey strut with respect to the vertical was fixed by manually sweeping the strut to the selected angle between 5 deg (swept upstream) and -15 deg (swept downstream) and locking the strut in position. In the present test, the sweep angle of the strut was set at -6.5 deg to allow surveys to be made as far aft on the model as XSTA = 37 in.

A sketch of the survey probe rake is shown in Fig. 4b. The top and rear surfaces of the rake were designed to mate to the Z' drive strut of the X-Z Survey Mechanism. The rake was provided with four 0.10-in. I.D. tubes through which were mounted the hot-wire anemometer and pitot pressure probes. One tube was used in the present test for housing a "touch-sensor" probe that caused the survey mechanism to halt when the probe made contact with the model surface. The tubes were fitted with clamps attached to the rake to hold the probes in position. One of the probe tubes of the rake was located in a removable section. This feature facilitated the replacement of fragile probes and allowed for critical probe alignments to be made under a laboratory microscope, as required for the hot-wire probe.

2.4 FLOW-FIELD SURVEY PROBES

The hot-wire anemometer probes (Fig. 5a) were fabricated by AEDC. Platinum, 10-percent-rhodium wires, drawn by the Wollaston process, of 20-micro-in. nominal diameter and approximately 140 diameters in length were attached to sharpened 3-mil nickel wire supports using a bonding technique developed by Philco-Ford Corporation (Ref. 11). The wire supports were inserted in an alumina cylinder of 0.032-in. diameter and 0.25-in. length, which was, in turn, cemented to an alumina cylinder of 0.093-in. diameter and 3.0-in.

8

length that carried the hot-wire leads through the probe holder of the survey mechanism.

The pitot pressure probe (Fig. 5b) had a cylindrical tip of 0.007-in. inside diameter. This probe was fabricated by cold-drawing a stainless steel tube through a set of wire-drawing dies until the desired inside diameter was obtained. The outside surface of the drawn tube was subsequently electropolished to a diameter of 0.015 in. to minimize interference with the flow field surveyed.

In addition to the probes used for survey measurements, a "touch-sensor" probe was used to halt the probe drive mechanism prior to contact of the other probes with the model. (See Sections 2.3 and 3.1.) The probe was made by brazing a lead wire to a piece of 0.031-in.-O.D. steel tubing. This tubing was telescoped in a larger diameter tube (0.093-in. O.D.) and electrically isolated from the larger tube using Pyroceram® cement. The inner tubing was bent to make contact with the model surface as required. A similar "touch-sensor" wire was attached to the probe shield (Section 2.3) to stop the probe drive mechanism prior to contact of the shield with the model. (See Section 3.1.)

2.5 TEST INSTRUMENTATION

2.5.1 Standard Instrumentation

The measuring devices, recording devices, and calibration methods for all parameters measured during this test are listed in Table 2. Also, Table 2 identifies the standard wind tunnel instruments and measuring techniques used to define test parameters such as the model attitude, the model surface conditions, probe positions, and probe measurements. Additional special instrumentation used in support of this test effort is discussed in the succeeding subsections.

2.5.2 Model Surface Instrumentation

The locations of the model instrumentation are listed in Table 1. The surface pressure orifices (TAP 1 - TAP 26) on the model had a diameter of 0.040 in.; and the pressures were measured using one-psid Druck® transducers or 2.5 psid ESP transducers included in the Tunnel B Standard Pressure System.

Coaxial surface thermocouple gages were used to measure the model surface heating rates and surface temperatures. The coax gage consists of an electrically insulated Chromel® center enclosed in a cylindrical Constantan sleeve. After assembly and installation in the model, the gage materials are blended together with a file creating thermal and electrical contact in a thin layer at the surface of the gage. The gage is used to monitor the surface temperature time history at a rate of 15 points per second. Assuming the surface thermocouple behaves as a homogeneous, one-dimensional, semi-infinite solid, its temperature time history can be used to define the corresponding time history of the incident heat flux. A complete description of this gage and the

data reduction procedure can be found in Refs. 12 and 13. The recording and calibrating procedures for this type gage are summarized in Table 2.

2.5.3 Hot-Film Anemometry Instrumentation

Flow fluctuation measurements were made using hot-wire anemometry techniques. Constant-current hot-wire anemometer instrumentation with auxiliary electronic equipment was furnished by AEDC. The anemometer current control (Philco-Ford Model ADP-13) which supplies the heating current to the sensor is capable of maintaining the current at any one of 15 preset values individually selected using push-button switches. The anemometer amplifier (Philco-Ford Model ADP-12), which amplifies the wire-response signal, contains the circuits required to compensate the signal electronically for thermal lag which is a characteristic of the finite heat capacity of the sensor. A square-wave generator (Shapiro/Edwards Model G-50) was used in determining the time constant of the sensor whenever required. The sensor heating current and mean voltage were fed to autoranging digital voltmeters for a visual display of these two parameters and to a Bell and Howell Model VR3700B magnetic tape machine and to the tunnel data system for recording. The sensor response a-c voltage was fed to an oscilloscope for visual display of the raw signal and to a wave analyzer (Hewlett-Packard Model 8553B/8552B) for visual display of the spectra of the fluctuating signal and was recorded on magnetic tape for subsequent analysis by AEDC. A detailed description of the hot-wire anemometer instrumentation is given in Ref. 14.

The a-c response signal from the hot-wire anemometer probe was recorded using the Bell and Howell Model VR3700B magnetic tape machine in the FM-WBII mode. This channel, when properly calibrated and adjusted, has a signal-to-noise ratio of 35 db at 1-v rms output and a frequency response of +1 to -3 db over a frequency range of 0 to 500 kHz. A sine wave generator was used to check each channel at several discrete frequencies, using an rms-voltmeter which was periodically calibrated on the 1-, 10-, and 100-v ranges. The sensor heating current and mean voltage signals from the hot-wire anemometer were also tape-recorded, using the FM-WBI mode. Magnetic tape recordings were made with a tape speed of 60 or 120 in./sec.

2.5.4 Pitot Probe Pressure Instrumentation

Pitot probe pressures were measured during surveys of the model boundary layer using a 15-psid Druck transducer calibrated for 10-psid full scale. As the probe was moved across the boundary layer, the small size of the pitot probe (Section 2.4) required a time delay between points in order to stabilize the pressure within the probe tubing between orifice and transducer. In order to reduce the lag time, the pitot pressure transducer was housed in a water-cooled package attached to the trailing edge of the strut on which the probe rake was mounted (Section 2.3). The distance between orifice and transducer was approximately 18 inches. The resultant lag time was about one second.

3.0 TEST DESCRIPTION

3.1 TEST CONDITIONS AND PROCEDURES

A summary of the nominal test conditions is given below.

M	PT, psia	TT, °R	V, ft/sec	Q, psia	T, °R	P, psia	RE/FT x 10^{-6}
7.94	225	1,310	3,855	1.06	98	0.024	1.0
7.96	340	1,310	3,857	1.58	98	0.036	1.5
7.98	453	1,310	3,859	2.10	97	0.047	2.0

A summary of the test runs for the present investigation using the cooled-wall hollow cylinder model is given in Table 3. Only heat-transfer data were acquired at RE/FT = 2.0 million.

In the continuous-flow Tunnel B, the model is mounted on a sting support mechanism in an installation tank directly underneath the tunnel test section. The tank is separated from the tunnel by a pair of fairing doors and a safety door. When closed, the fairing doors, except for a slot for the pitch sector, cover the opening to the tank, and the safety door seals the tunnel from the tank area. After the model is prepared for a data run, the personnel access door to the installation tank is closed, the tank is vented to the tunnel flow, the safety and fairing doors are opened, the model is injected into the airstream, and the fairing doors are closed. After the data are obtained, the sequence is reversed; the model is retracted into the tank which is then vented to atmosphere to allow access to the model in preparation for the next run. The sequence is repeated for each configuration change.

Probes mounted to the X-Z mechanism (Section 2.3) are deployed for measurements by the following sequence of operations: the air lock is closed, secured over the mechanism, and evacuated; and the access door to the tunnel test section is opened. The various drive systems are used to inject the probes into the test section and position the probes at a designated survey station along the length of the model, the shield protecting the probes is raised exposing them to the flow, and the flow field is traversed to selected probe heights. When the traverse has been concluded, the shield is closed over the probes, and the mechanism is repositioned along the model. When the surveys are completed or when a probe is to be replaced, the X-Z Mechanism is retracted from the flow, and the test section access door is closed. The air lock is then opened to allow personnel access to the mechanism.

The survey probe height relative to the model was monitored using a high-magnification, closed-circuit television (CCTV) system. The video camera was fitted with a telescopic lens system which gave a magnification factor of 20 for the monitor image. The probe and model were back-lighted using the collimated light beam from the Tunnel B

11

shadowgraph system which produced high-contrast silhouettes of the model and probe (Fig. 6). The camera was mounted on a horizontal-vertical traversing mount to facilitate alignment of the camera with the probe at various model stations visible through the test section windows. The video camera was interfaced with an image analyzer/digitizer system which was used to measure the distance between the probe and model surface using computer-assisted image analysis techniques. For each measurement the lower edge of the probe and the upper edge of the model surface were located by an operator using a cursor with the video image. The system was calibrated prior to testing by the same operator using the same technique to locate edges separated by a known distance.

A hardcopy of the video image of the probes and model edge was provided in near real-time, showing, by means of a graphics line, the location of the edges measured and displaying a printout of the measured distance and other pertinent information. The accuracy of this measurement technique was determined to be better than ±0.0007 in. over a range of 0.003 to 0.2 in. under air-off conditions. The video images used for test measurements were recorded on disk for post test review, if needed.

The flow-field surveys were accomplished in the following sequence: (1) the survey mechanism was positioned at the desired model axial station (XSTA) by the controller operating in either manual or automatic mode and locked in axial position, (2) the survey mechanism was driven downward toward the surface by the controller until the "touch-sensor" wire (Section 2.4) attached to the probe shield made contact with the model surface, (3) final adjustments of probe instrumentation were made and the shield was raised, (4) the survey mechanism was driven toward the model surface by the controller until the "touch-sensor" probe (Section 2.3) made contact with the surface, (5) measurements of probe positions relative to the surface and to each other were made using the image analyzer and the information was manually entered into the data system, (6) the probes were traversed across the flow field in selected increments by the controller in either manual or automatic mode to acquire the desired data, (7) the axial position of the survey mechanism was unlocked and the mechanism was repositioned at the next survey station along the model.

3.2 DATA ACQUISITION

The primary test technique used in the present investigation of the development of instabilities in a laminar boundary layer was hot-wire anemometry. In addition, mean-flow boundary-layer profile data (pitot pressure profiles) were acquired in order to define the flow environment in the vicinity of the hot-wire. All boundary-layer measurements were made above the top (zero) ray of the model. Surface pressures and temperatures on the model were measured to supplement the profile data. The various types of data acquired are summarized in Table 3. Model stations for surveys are also listed in Tables 3a and 3b.

3.2.1 Hot-Wire Anemometry Data

The hot-wire anemometer data acquired during the present testing were of two general categories: (1) continuous-traverse surveys of the boundary layer to map the response of the hot-wire anemometer as a function of distance from the surface and (2) discrete-point hot-wire measurements using the wire operated at one or two wire heating currents at one or more locations on a profile.

Data of the first category were acquired with the hot wire operated using a single heating current, in the present case the maximum (practical) current. The probe was generally translated in a continuous manner from near the model surface outward beyond the edge of the boundary layer. These data were recorded as analog plots of the hot-wire response (rms of the a-c voltage component) versus probe height above the model surface. The plot was used primarily for the purpose of determining the station in the boundary-layer profile where the hot-wire output reached a maximum value.

Discrete-point hot-wire data (second category) were acquired at locations determined from the continuous-traverse surveys (first category data). The point of maximum rms voltage output of the hot wire, the "maximum energy point" of the profile, was selected for quantitative measurements at each model station. The quantitative data were acquired using each of two wire heating currents; one current was nominal-zero to obtain a measurement of the electronic noise of the anemometer instrumentation. The other current was the maximum (practical) current. Each wire heating current, wire mean voltage (d-c component) and the rms value of the wire voltage fluctuation (a-c component) were measured 40 times using the Tunnel B data system. At the same time, the hot wire parameters were recorded (generally, a five-second record duration) on magnetic tape with a tape transport speed of 120 in./sec.

Discrete-point hot-wire data were also obtained simultaneously with the boundary-layer profile data (Section 3.2.2). In this case a measurement and recording of the electronic noise was made only at the start of the traverse and was assumed to be valid for all points of the profile. The tape recording duration was 5 sec and a tape transport speed of 60 in./sec was used.

3.2.2 Profile and Surface Data

Mean-flow boundary-layer profiles extended from a height of 0.05 in. above the model surface to a distance of 1.5 times the boundary-layer thickness. A profile typically consisted of 47 data points (heights). The probe direction of travel was at an angle of 6.5 deg with respect to the vertical (Section 2.3).

Model surface pressures, temperature distributions, and heat-flux distributions were acquired to supplement the boundary-layer surveys. The surface pressures and temperatures were obtained throughout the test.

3.3 DATA REDUCTION

3.3.1 Hot Wire Anemometer Data

In the present discussion, as it pertains to the reduction of hot-wire anemometer data, only the basic measurements tabulated in the data package that accompanies this report will be considered. (Examples of the tabulations are shown in the Sample Data.) The data processing associated with spectral analysis, modal analysis, and determination of amplification rates of laminar disturbances is beyond the scope of this report. However, extended data reduction of the present hot-wire results to achieve these analyses is planned.

The basic measurements associated with quantitative hot-wire data are the following: wire heating current (CURRENT), wire mean voltage (EBAR), and the rms value of the wire fluctuating response voltage (ERMS). The average value of 40 measurements of each of the three parameters was determined for each nominal wire heating current employed, and the results were tabulated under the designation "DATA TYPE 9" together with certain associated model, flow field, and tunnel conditions. (See Sample 1.)

3.3.2 Flow-Field Survey Data

The mean flow-field data reduction ("DATA TYPE 4") included calculation of the local Mach number and other local flow parameters, determination of the height of each probe relative to the model surface, definition of the boundary-layer total thickness, and evaluation of the displacement and momentum thicknesses. Sample tabulated data are shown in Sample 2, and typical plotted results are shown in Fig. 7. The data reduction procedures are outlined as follows.

The local Mach number in the flow field around the model was determined using the measured pitot pressure (PP) and the model static pressure (PWL). The total temperature distribution across the boundary layer on the cooled-wall hollow cylinder was calculated, using a computer code (Ref. 15), as a function of local Mach number. The normalized distribution used is shown in Fig. 8. In earlier tests of this type with cone models (Refs. 1-4), the total temperature distribution across the boundary layer was measured using an unshielded thermocouple probe. Attempts to use a similar probe in the present measurements in conjunction with the hot-wire probe and pitot pressure probe resulted in an unacceptable mutual interference among the probes.

The height of each probe above the model surface, in the normal direction, was calculated for each point in a given flow-field survey, taking into consideration the following parameters: the initial vertical distance determined from the CCTV image, the distance traversed from the initial position employing the survey probe drive, the sweep angle of the survey strut, the lateral displacement of the probe from the vertical plane of symmetry of the model, and the radius of the model.

14

3.3.3 Model Surface Pressure and Temperature Data

Model surface pressures and temperatures were tabulated under the designation "DATA TYPE 2" and "DATA TYPE 4." The data presented as DATA TYPE 2 (see Sample 3) represent a single measurement of each pressure and each temperature. These data were, in general, acquired when the survey probes were positioned to minimize interference with the surface measurements at $X \leq 37$ in.

Model surface measurements were also included among the DATA TYPE 4 results. In this case, surface conditions were measured each time that probe data were acquired. The surface data presented in these tabulations represent the average of the 47 values measured at each orifice and each thermocouple. It should be noted that pressures along the 15-, 90-, and 270-deg rays were often influenced by the presence of the survey probes and the Z' survey strut. The extent of the influence was governed by the location of the probes above the model. It is recommended in general that only the pressures measured along the 180-deg ray be used from the surface data tabulated under DATA TYPE 4.

Measured pressure distributions are shown in Fig. 9 for the two test conditions RE/FT = 1.0 and 1.5 million. For the former case (Fig. 9a), the mean value of the surface pressures (at THETA = 15, 90, and 270 deg) is approximately PW/P = 1.1. For the case of RE/FT = 1.5 million (Fig. 9b), the mean value is essentially PW/P = 1.0. In either case, the estimated measurement uncertainty band associated with the ratio PW/P is relatively wide. It was desired to have within the uncertainty band a systematic relationship between PW/P and X for use in specifying the surface pressure PWL to be employed in the boundary-layer calculations at a given X station and RE/FT. The following procedure was used to develop such a relationship: (1) It was assumed that the Mach number ME at the edge of the boundary layer did not vary significantly with X along the region of surveys and was equal to the test-section free-stream Mach number, and (2) The pitot pressure PPE at the edge of the boundary-layer was used with this Mach number (ME) and the Rayleigh pitot equation to calculate the value of PWL. The resultant variation of PWL/P _versus_ X is represented by the sloped line in each of the Figs. 9a and 9b.

3.3.4 Heat-Transfer Data

The coax gage heat flux at each instrumented location was computed for each time point (t_n) from the measured surface temperature by the following equation derived from semi-infinite solid considerations

$$QDOT(t_n) = \frac{2C\left(t_n\right)}{\sqrt{\pi}} \sum_{j=1}^{n} \frac{TW\left(t_j\right) - TW\left(t_{j-1}\right)}{\sqrt{t_n - t_j} + \sqrt{t_n - t_{j-1}}} \tag{1}$$

The coax gage surface temperature, TW (t_j), was computed from the thermocouple millivolt output using a curve fit to thermocouple

reference tables. The value of the coefficient C (t_n) was an effective scale factor for the coax gage which was calculated from

$$C\left(t_n\right) = 5.26 \, x \, 10^{-4} \left[\frac{TW\left(t_n\right) + TW\left(t_1\right)}{2} \right] + 0.12688 \qquad (2)$$

which accounts for the density, specific heat, and thermal conductivity of the gage materials.

To reduce the effects of any noise in the gage output, the values of QDOT were averaged for fifteen consecutive readings after the test article reached the tunnel centerline. The gage surface temperature was also averaged for the heat-transfer data.

An example of the tabulated heat-transfer data is shown in Sample 4.

3.4 MEASUREMENT UNCERTAINTIES

In general, instrumentation calibrations and data uncertainty estimates were made using methods presented in Ref. 16. Measurement uncertainty (U) is a combination of bias and precision errors defined as

$$U = \pm \left(B + t_{95} S \right)$$

where B is the bias limit, S is the standard deviation, and t_{95} is the 95th percentile point for the two-tailed Student's "t" distribution, which equals approximately 2 for degrees of freedom greater than 30.

Estimates of the measured data uncertainties for this test are given in Table 2. In general, measurement uncertainties are determined from in-place calibrations through the data recording system and data reduction program. The propagation of the estimated bias and precision errors of the measured data through the data reduction was determined for free-stream parameters in accordance with Ref. 16, and is summarized in Table 4.

4.0 DATA PACKAGE PRESENTATION

Basic hot-wire anemometer data, boundary-layer profile data, and model surface data from the test were reduced to tabular and graphical form for presentation as a Data Package. Examples of the basic data tabulations are shown in the Sample Data.

REFERENCES

1. Siler, L. G. and Donaldson, J. C. "Boundary-Layer Measurements on Slender Blunt Cones at Free-Stream Mach Number 8." AEDC-TSR-79-V71 (AD-A085712), December 1979.

2. Donaldson, J. C. and Simons, S. A. "Investigation of the Development of Laminar Boundary-Layer Instabilities Along a Sharp Cone." AEDC-TSR-85-V16 (AD-A159370), April 1985.

3. Donaldson, J. C. and Simons, S. A. "Investigation of the Development of Laminar Boundary-layer Instabilities Along a Blunted Cone." AEDC-TSR-86-V46, November 1986.

4. Donaldson, J. C. and Hatcher, M. G. "Investigation of the Development of Laminar Boundary-Layer Instabilities Along a Cooled-Wall Cone in Hypersonic Flows." AEDC-TSR-88-V32, December 1988.

5. Stetson, K. F., Thompson, E. R., Donaldson, J. C., and Siler, L. G. "Laminar Boundary-Layer Stability Experiments on a Cone at Mach 8, Part 1: Sharp Cone." AIAA Paper No. 83-1761, July 1983.

6. Stetson, K. F., Thompson, E. R., Donaldson J. C., and Siler, L. G. "Laminar Boundary-Layer Stability Experiments on a Cone at Mach 8, Part 2: Blunt Cone." AIAA Paper No. 84-0006, January 1984.

7. Stetson, K. F., Thompson, E. R., Donaldson J. C., and Siler, L. G. "Laminar Boundary-Layer Stability Experiments on a Cone at Mach 8, Part 3: Sharp Cone at Angle of Attack." AIAA Paper No. 85-0492, January 1985.

8. Stetson, K. F., Thompson, E. R., Donaldson J. C., and Siler, L. G. "Laminar Boundary-Layer Stability Experiments on a Cone at Mach 8, Part 4: On Unit Reynolds Number and Environmental Effects." AIAA Paper No. 86-1087, May 1986.

9. Stetson, K. F., Thompson, E. R., Donaldson, J. C., and Siler, L. G. "Laminar Boundary-Layer Stability Experiments on a Cone at Mach 8, Part 5: Tests with a Cooled Model." AIAA Paper No. 89-1895, June 1989.

10. Boudreau, A. H. "Performance and Operational Characteristics of AEDC/VKF Tunnels A, B, and C." AEDC-TR-80-48 (AD-A102614), July 1981.

11. Doughman, E. L. "Development of a Hot-Wire Anemometer for Hypersonic Turbulent Flows." Philco-Ford Corporation Publication No. U-4944, December 1971; and The Review of Scientific Instruments, Vol. 43, No. 8, August 1972, pp. 1200-1202.

12. Stallings, D. W., Matthews, R. K., and Jenke, L. M. "Recent Developments in Aerothermodynamic Test Techniques at the AEDC von Karman Gas Dynamics Facility." International Congress on Instrumentation in Aerospace Simulation Facilities, September 1979.

13. Cook, W. J. and Felderman, E. J. "Reduction of Data from Thin-Film Heat Transfer Gages: A Concise Numerical Technique." AIAA Journal, Vol. 4, No. 3, March 1966, p. 561.

14. Donaldson, J. C., Nelson, C. G., and O'Hare, J. E. "The Development of Hot-Wire Anemometer Test Capabilities for $M_\infty = 6$ and $M_\infty = 8$ Applications." AEDC-TR-76-88 (AD-A029570), September 1976.

15. Gasperas, G. "Effect of Wall Temperature Distribution on the Stability of the Compressible Boundary Layer." AIAA Paper No. 89-1894, June 1989.

16. Abernethy, R. B. et al., and Thompson, J. W. "Handbook Uncertainty in Gas Turbine Measurements." AEDC-TR-73-5 (AD755356), February 1973.
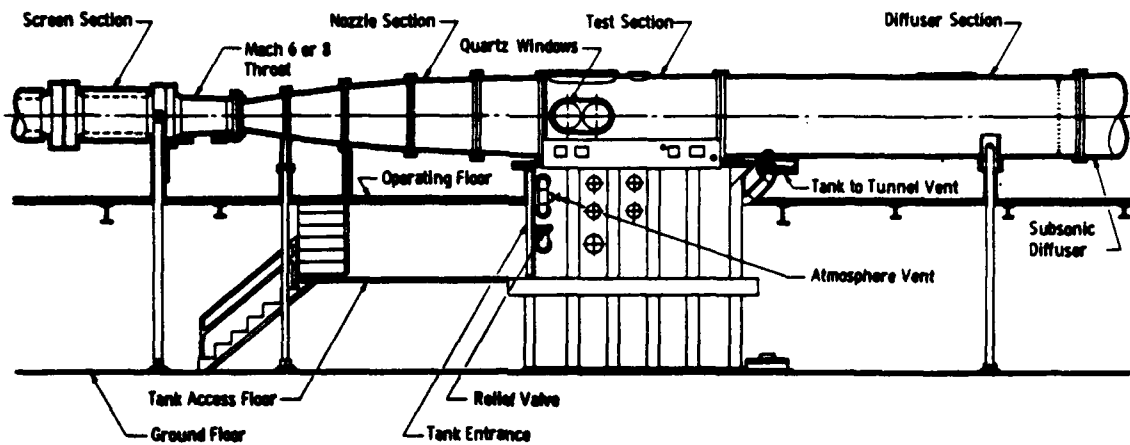
a. Tunnel assembly
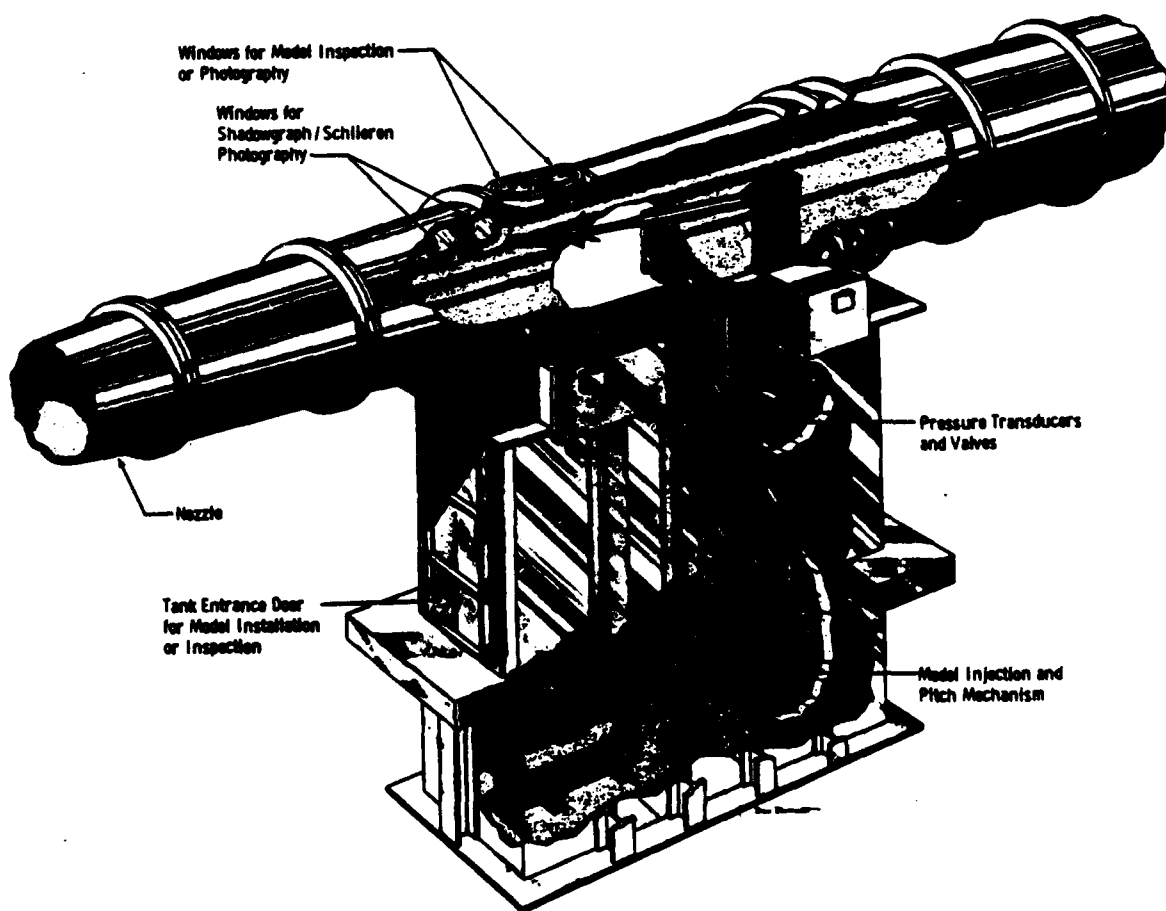
b. Tunnel test section

Figure 1.   AEDC Hypersonic Wind Tunnel B

19

All dimensions
are in inches.

Hollow Cylinder

Supporting Collar

Model

Sting
(Water Jacket Omitted)

59.50

7.50

O.D. = 10.72

XSTA
37.00

XSTA
10.00

3.74

O.D. = 10.00
I.D. = 8.10

Leading Edge
Section

X > 0

Figure 2. Model Geometry

20

Survey Rake
(Shield Lowered)

Shield Touch Sensor

Hollow Cylinder Model
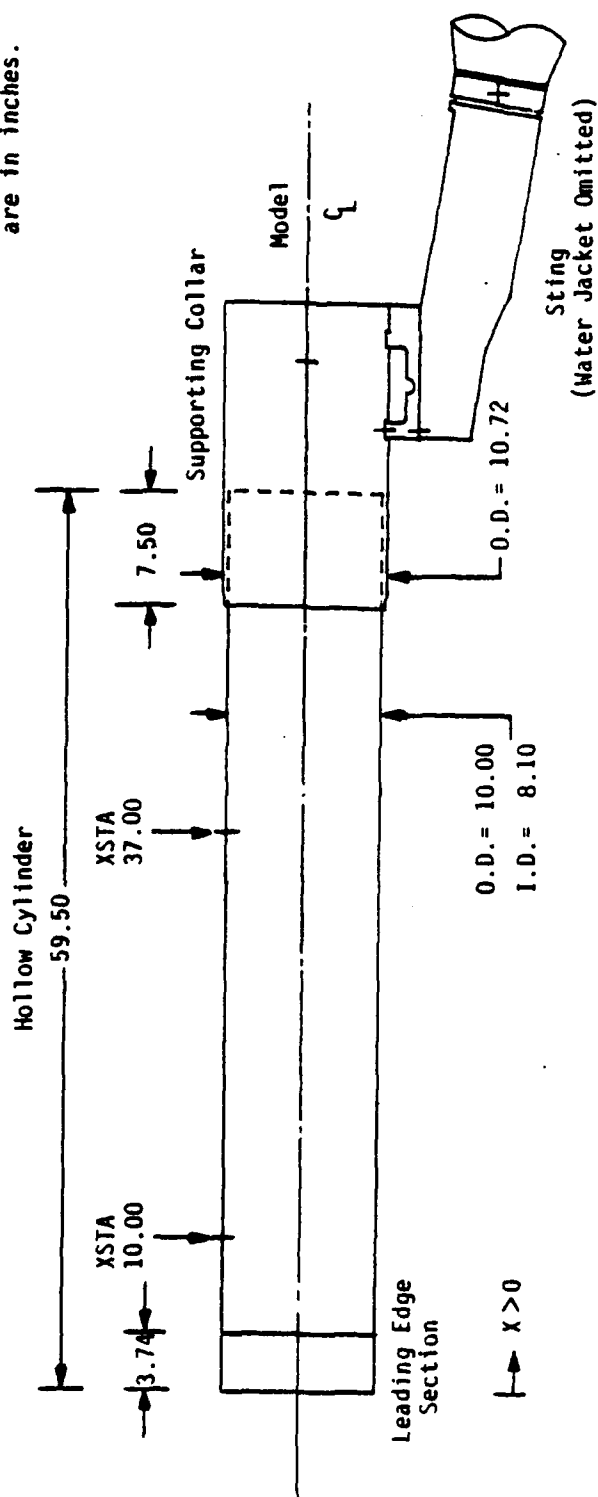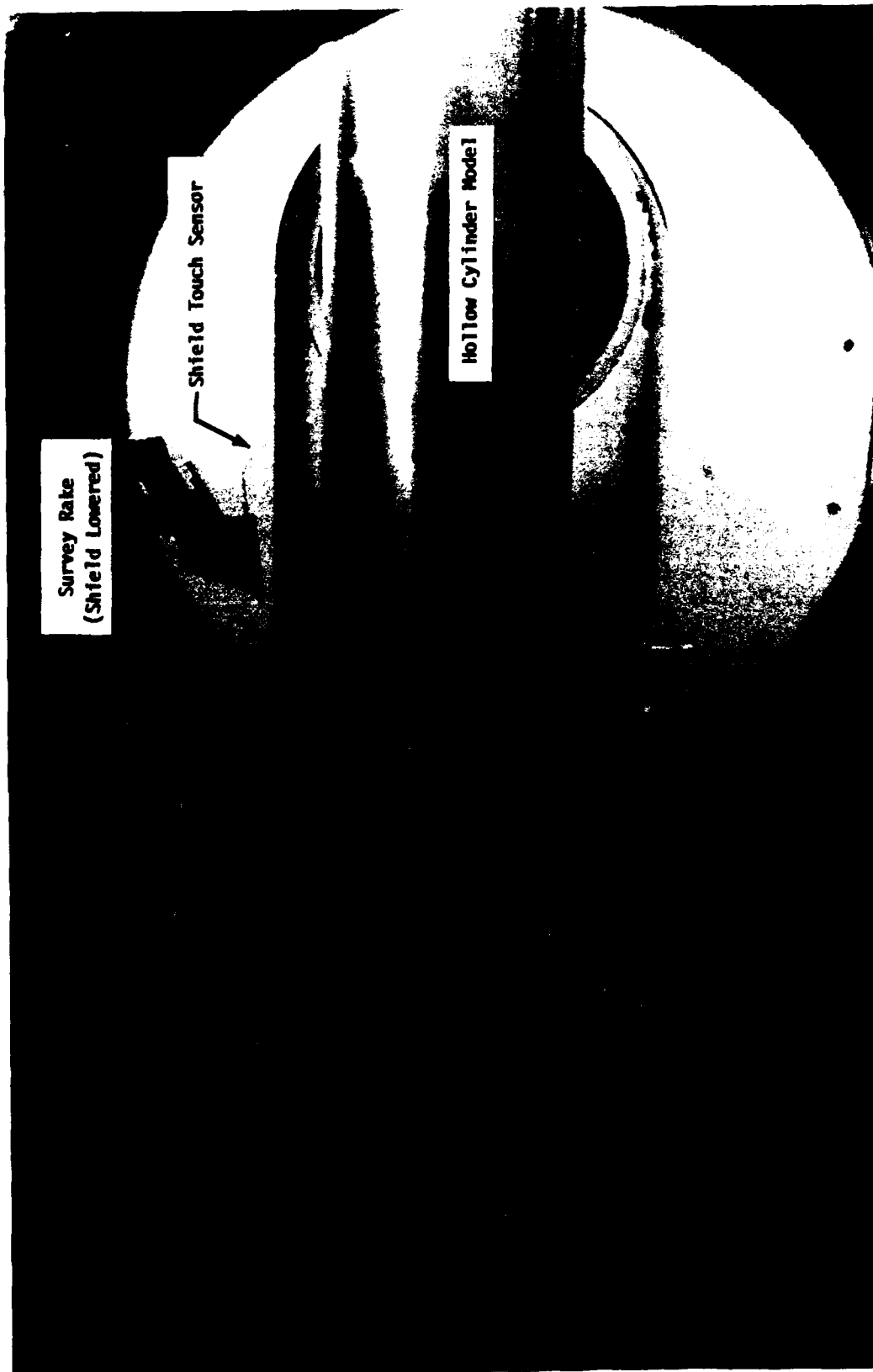
Figure 3. Test Installation

Housing for Pitot Pressure Transducer Package

Instrumentation Leads

Z' Drive Strut

Probe Shield (Raised Position)
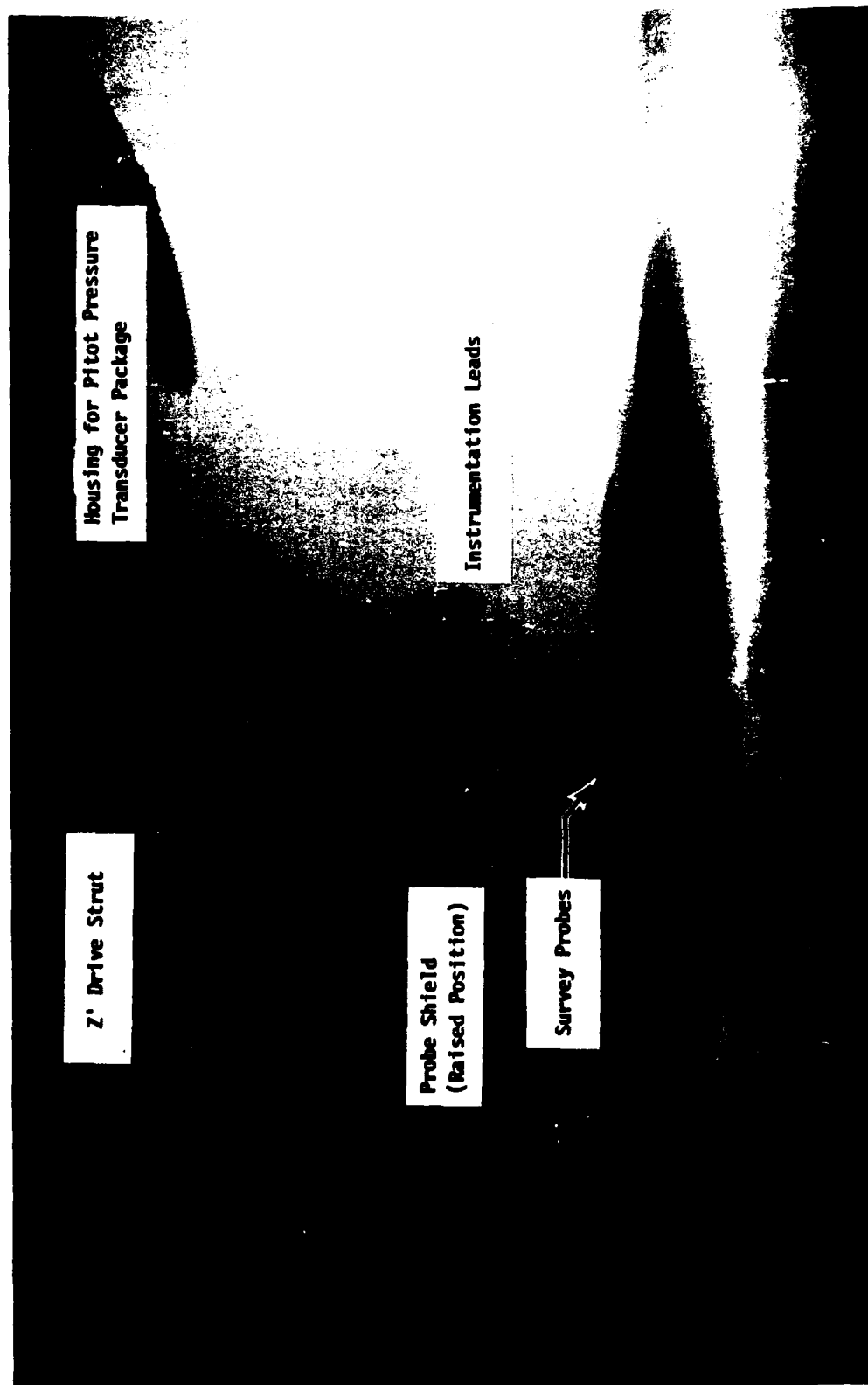
Survey Probes

a. Survey Rake Installation

Figure 4. Survey Probe Rake

(Hot-Wire Probe Omitted
for Clarity)

Side View

Probe Clamps

Removable
Section

Perspective View

Hot-Wire Anemometer Probe
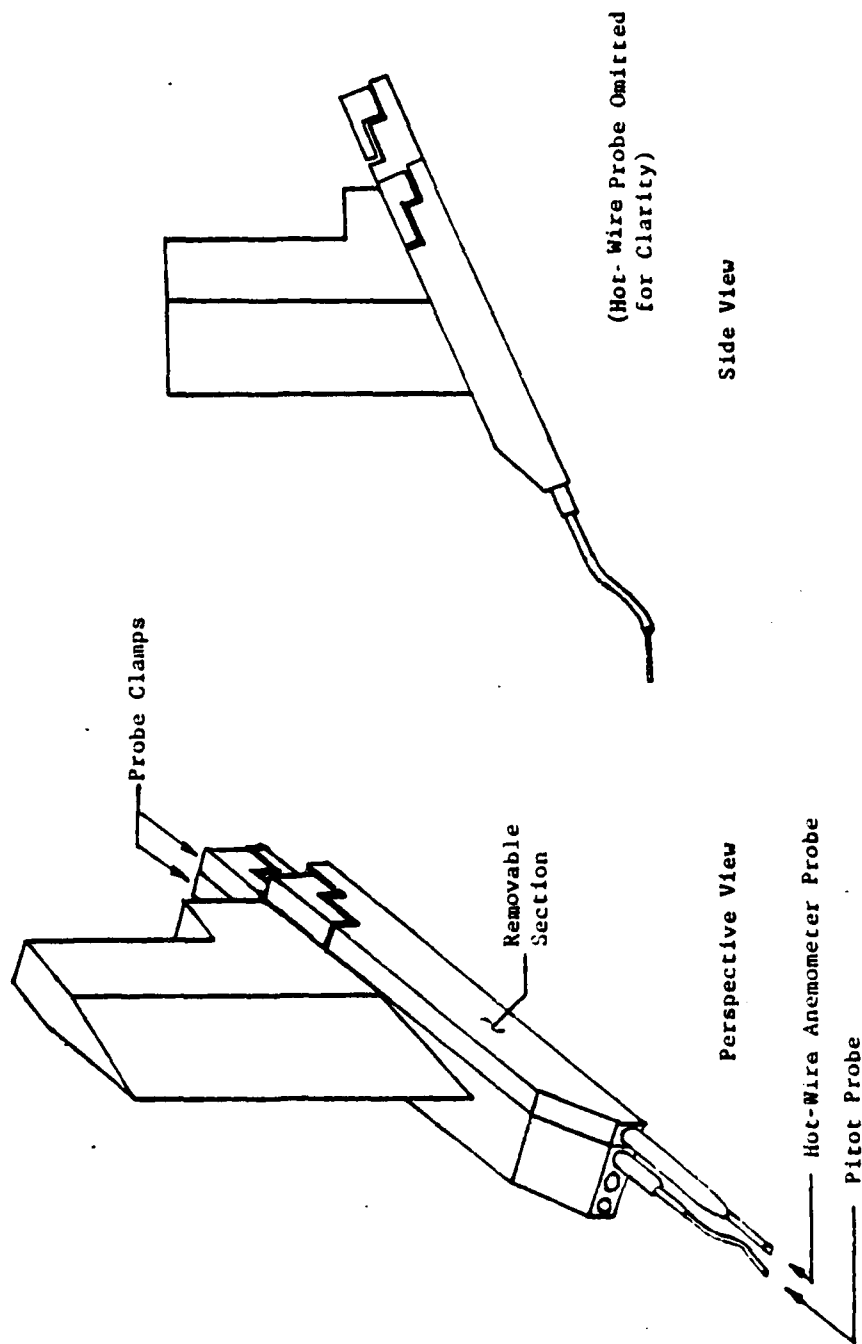
Pitot Probe

b. Survey Rake Details

Figure 4. (Concluded).

23

Pt-10% Rh
0.00002 in. diam.

sensor wire

sensor supports
0.003 in. diam.
nickel wire

copper leads

length ≃ 140 diam

alumina cylinder, 0.093 in. O.D.
(two bore)

epoxy fairing

alumina cylinder, 0.032 in. O.D. (two bore)

Pyroceram® fairing

a.   Hot-Wire Anemometer Probe

0.063 OD x 0.040 ID

0.093 OD x 0.063 ID

0.032 OD x 0.024 ID
304 SS

0.015 OD x 0.007 ID

All Dimensions in Inches
Not Drawn to Scale

0.20
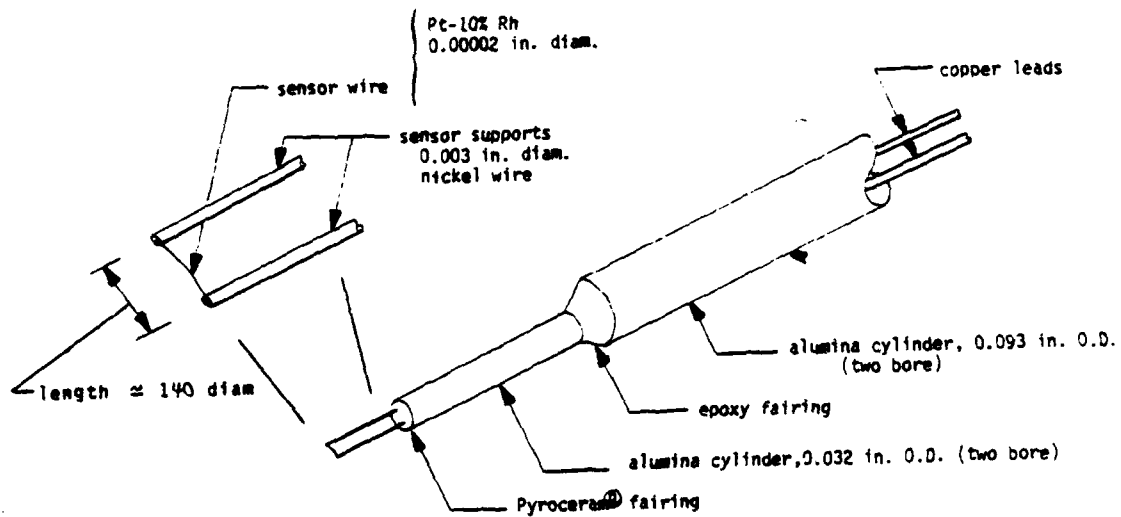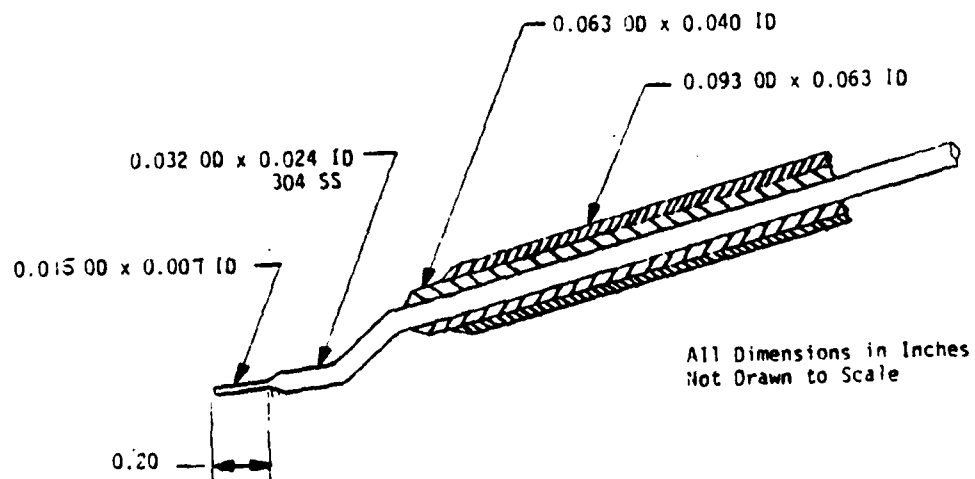
b.   Pitot probe

Figure 5.   Probe Details
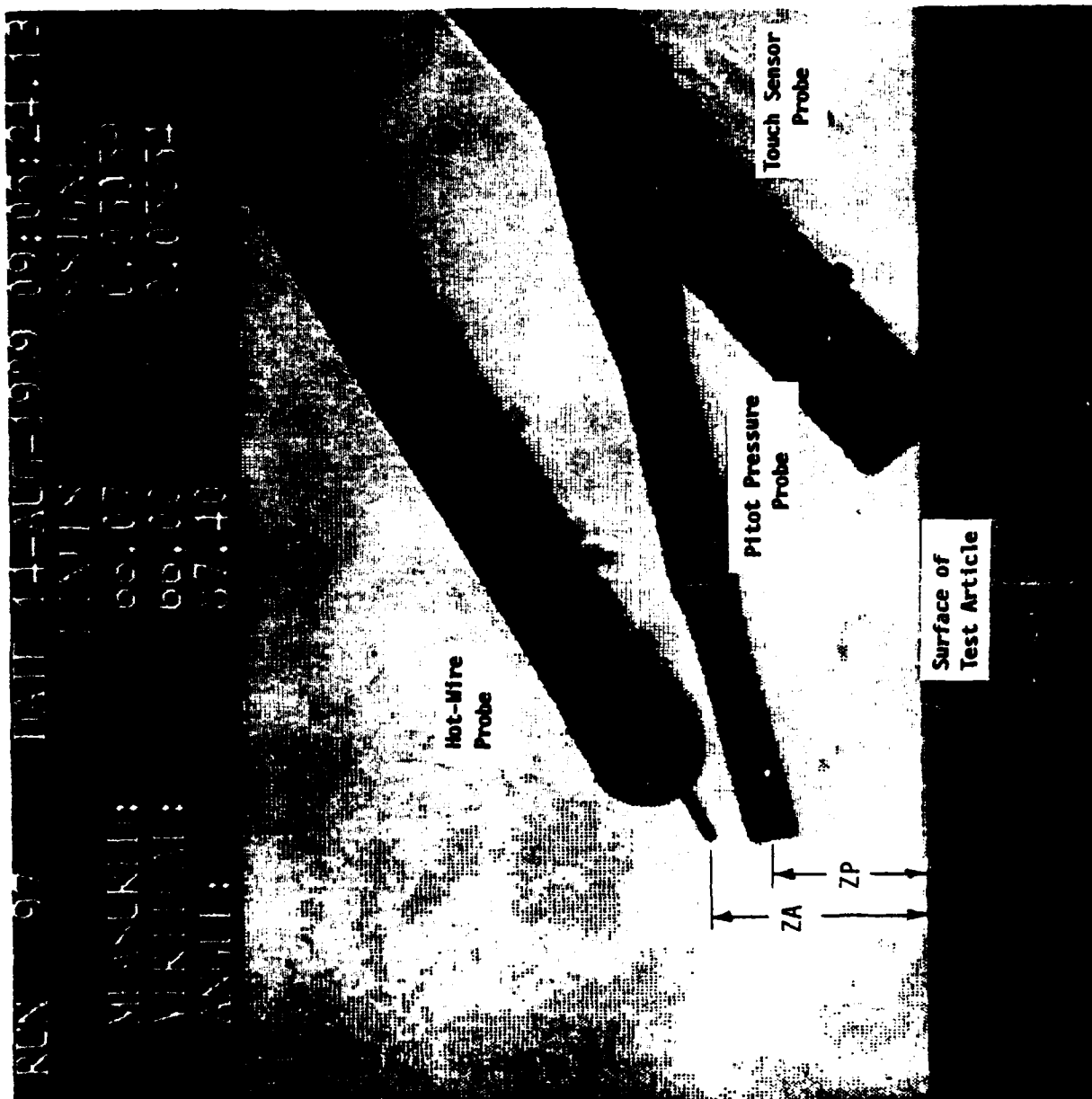
Figure 6. Video Image of Probe and Model Edges
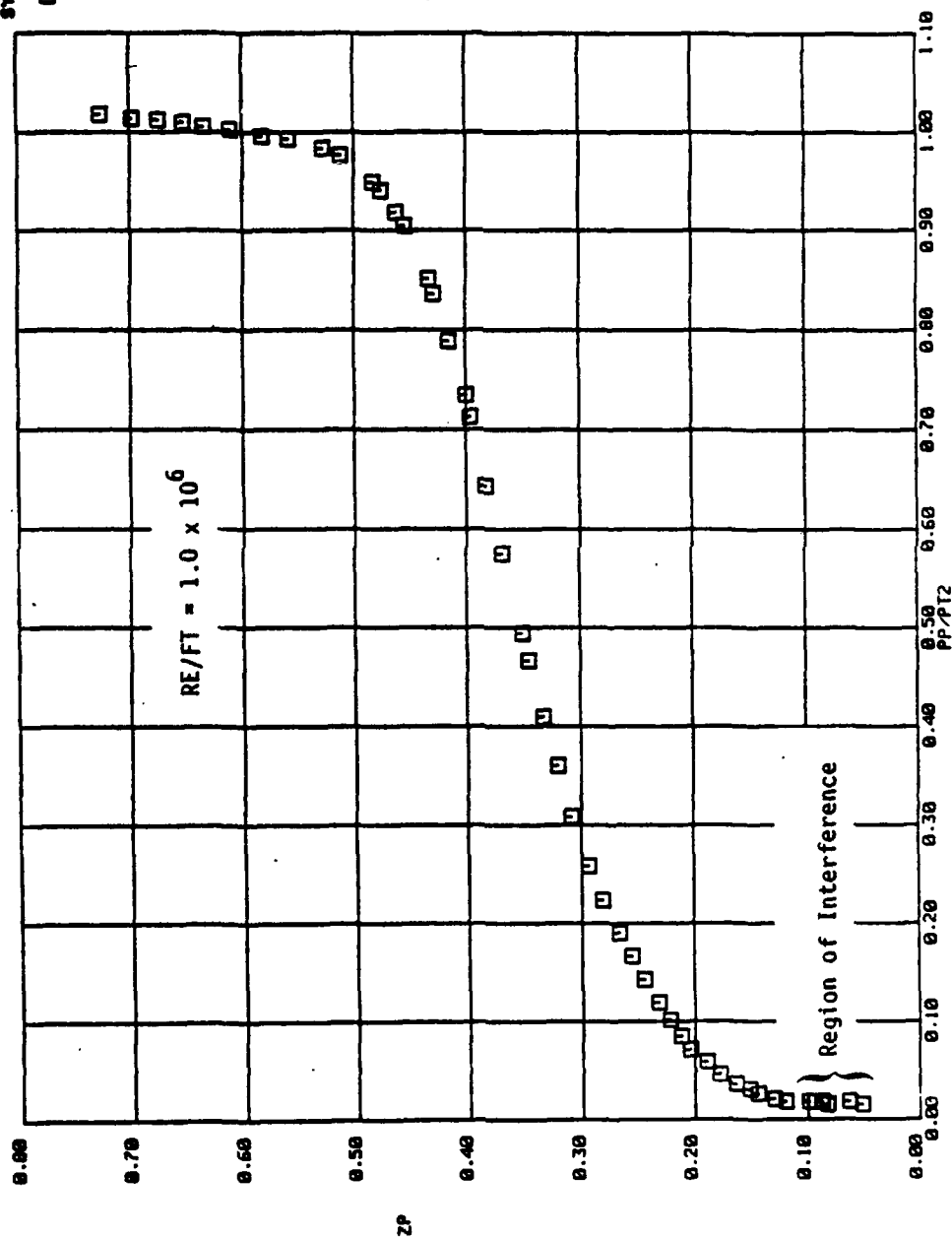
Figure 7. Typical Results of a Boundary-Layer Survey
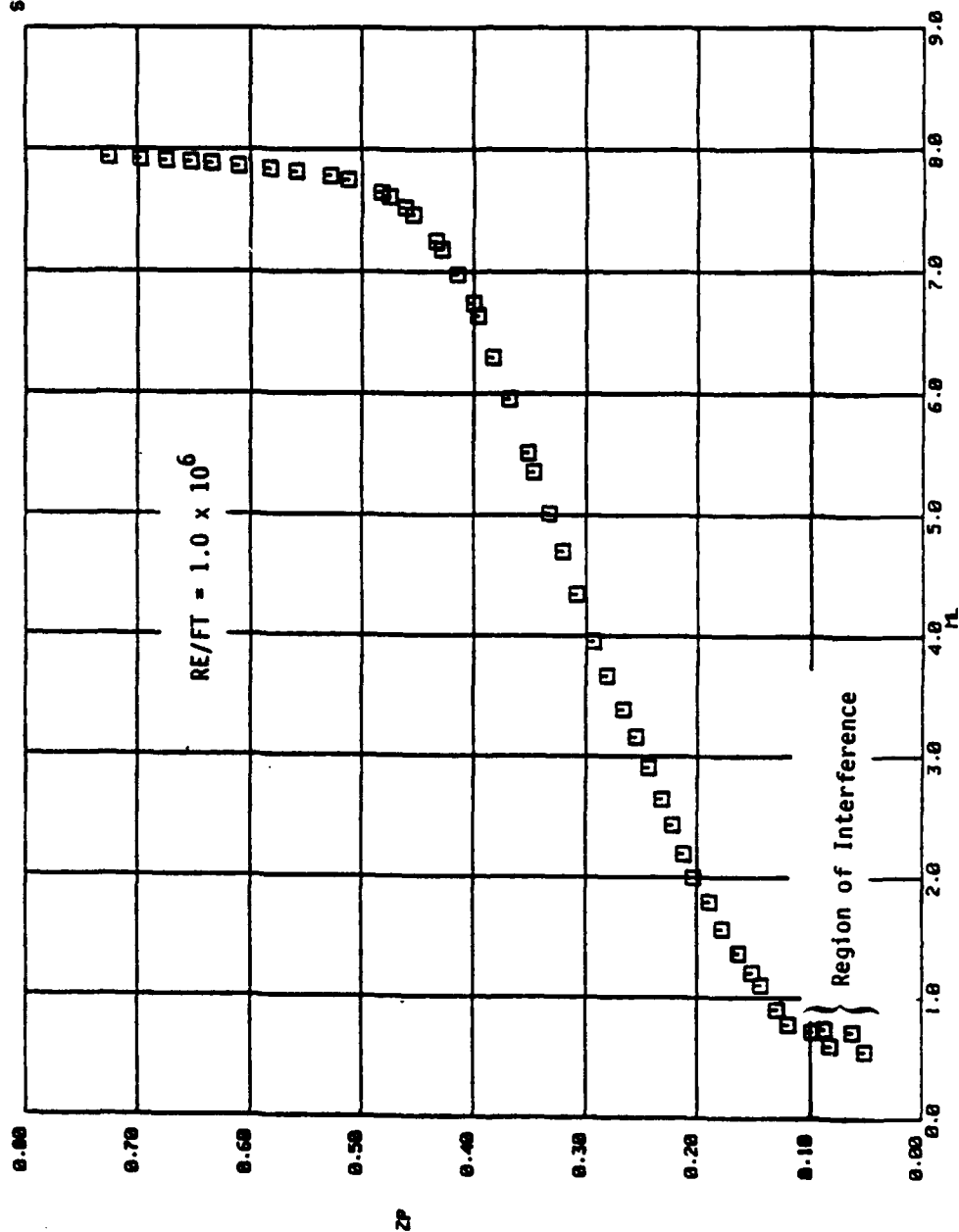
Figure 7. (Continued)
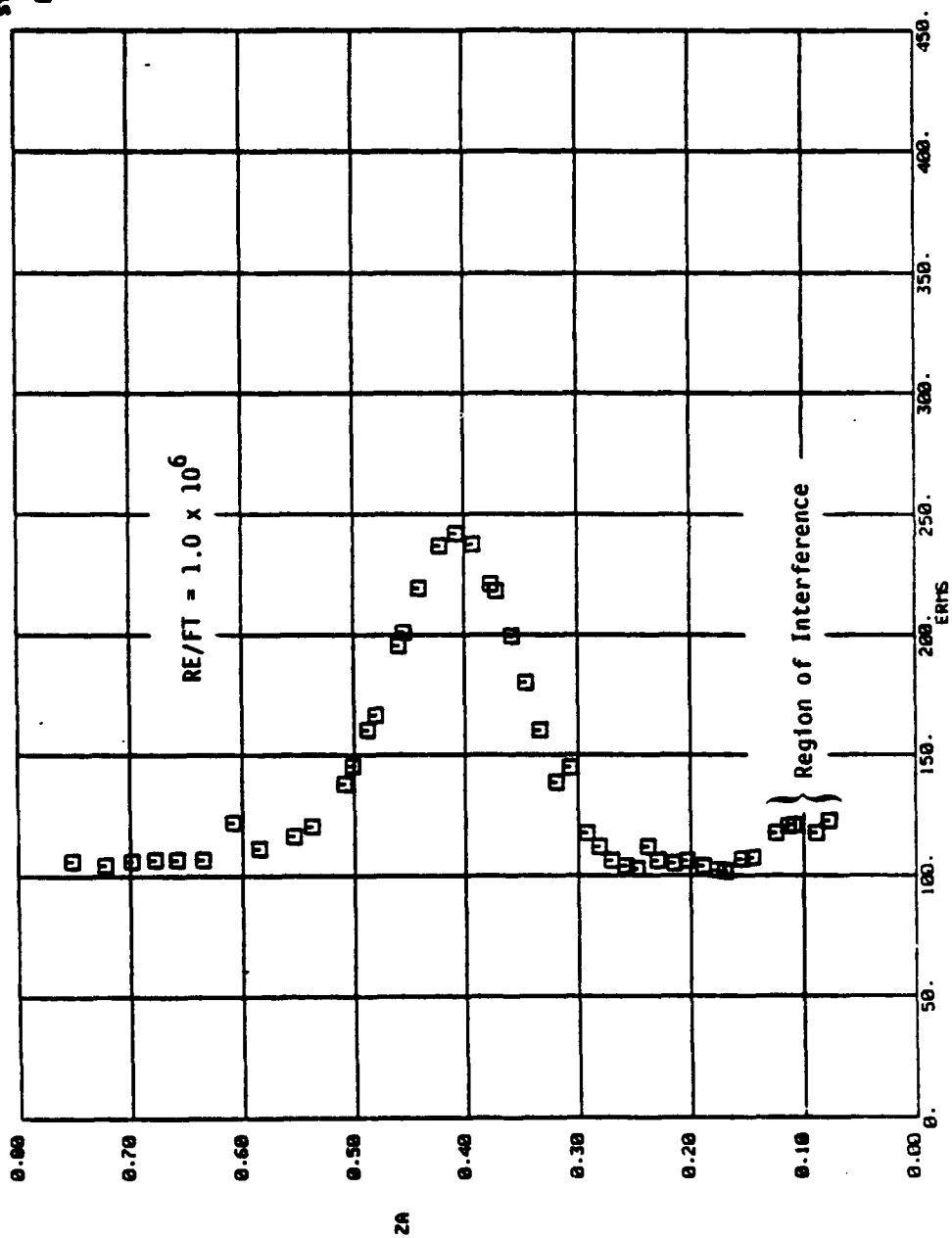
Figure 7. (Concluded)

28
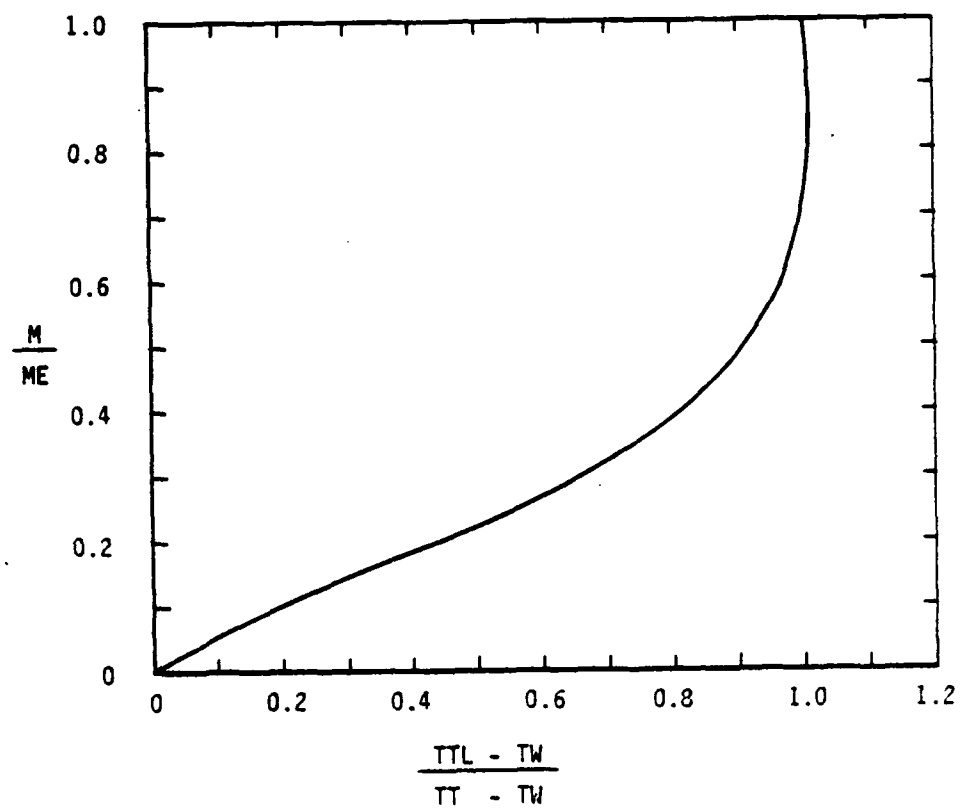
Figure 8. Computer-Generated Boundary-Layer Total Temperature Profile

THETA , deg

□	15
O	90
△	180
◇	270
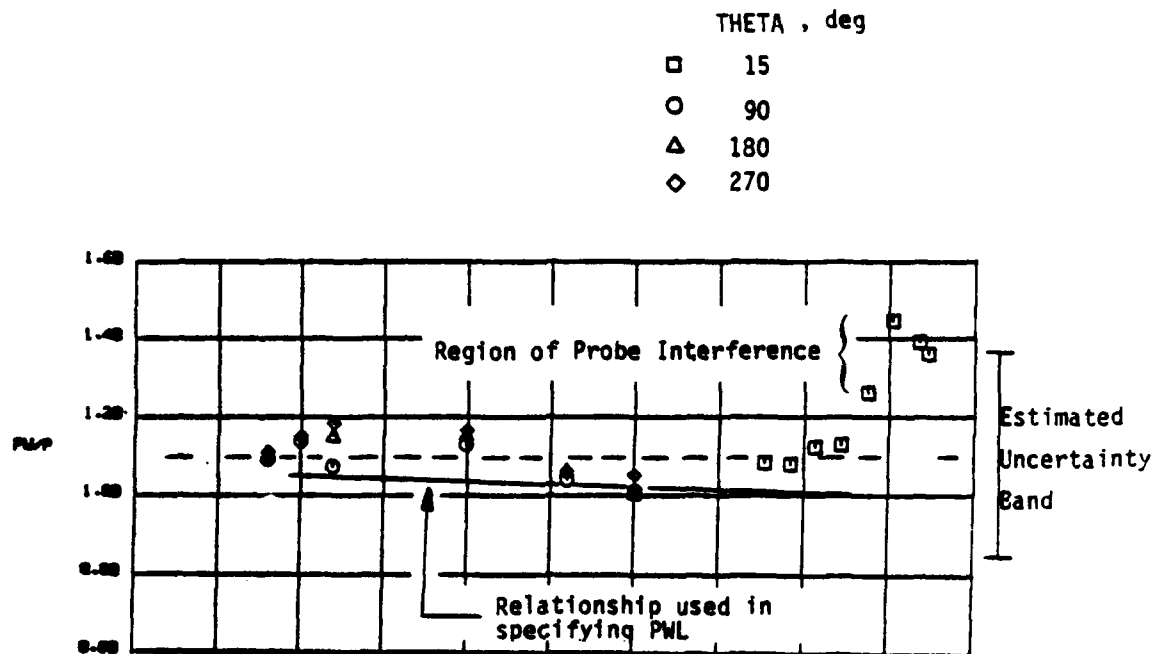
a.   RE/FT = 1.0 million
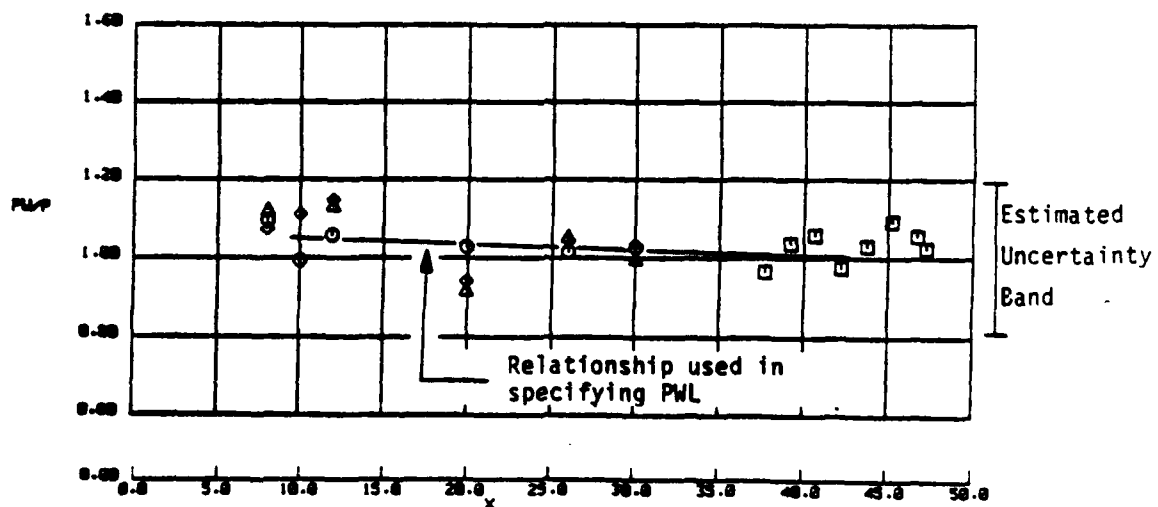
b.   RE/FT = 1.5 million

Figure 9.   Model Surface Pressure Distributions

30

TABLE 1. MODEL INSTRUMENTATION LOCATIONS

PRESSURE ORIFICE LOCATIONS			COAXIAL THERMOCOUPLE LOCATIONS		
TAP	X (in)	THETA (deg)	T/C	X (in)	THETA (deg)
1	37.721	15	1	6.996	345
2	39.215	15	2	7.982	345
3	40.712	15	3	15.980	345
4	42.224	15	4	16.978	345
5	43.709	15	5	17.983	345
6	45.216	15	6	19.972	345
7	46.728	15	7	21.966	345
8	47.226	15	8	22.988	345
9	7.973	90	9	23.981	345
10	9.971	90	10	24.966	345
11	11.973	90	11	25.966	345
12	19.969	90	12	26.975	345
13	25.971	90	13	27.966	345
14	29.973	90	14	28.970	345
15	7.970	180	15	29.964	345
16	9.971	180	16	31.966	345
17	11.968	180	17	32.969	345
18	19.971	180	18	33.964	345
19	25.974	180	19	34.954	345
20	29.969	180	20	35.964	345
21	7.970	270	21	36.970	345
22	9.967	270	22	37.969	345
23	11.966	270	23	38.957	345
24	19.970	270	24	39.958	345
25	25.971	270	25	40.958	345
26	29.973	270	26	41.956	345
			27	42.962	345

31

TABLE 2. ESTIMATED UNCERTAINTIES OF MEASURED PARAMETERS

Parameter Designation	Steady-State Estimated Measurement [a]								Range	Type of Measuring Device	Type of Recording Device	Method of System Calibration
	Precision Index (S)			Bias (B)		Uncertainty ± (B + t95S)						
	Percent of Reading	Unit of Measurement	Degree of Freedom	Percent of Reading	Unit of Measurement	Percent of Reading	Unit of Measurement					
Stilling Chamber Pressure (PT), psi		± 0.1 psi	>30		± 0.1 psi		± 0.3 psi		± 0 to 900 psi	Paroscientific Digiquartz Pressure Transducer	Digital data acquisition system	In-place application of multiple pressure levels measured with a pressure measuring device calibrated in the standards laboratory
Total Temperature (TT), °F		± 1 °F	>30		± 2°F		± 4 °F		32 to 530°F	Chromel-Alumel[*] Thermocouple	Digital Thermometer and Micro Processor Averaged (TTP) Digital Thermometer for Redundant (TTR)	Thermocouple verification of NBS conformity/voltage substitution calibration
		± 1 °F	>30	± 0.375		± (0.375	% + 2 °F)		530°F to 2300°F			
Angle of Attack (ALPHA), deg		± 0.025 deg	>30		0°		± 0.05 deg		± 15 deg	Potentiometer	Digital data acquisition system/analog-to-digital converter	Heidenhain rotary encoder ROD700 Resolution: 0.0006° Overall accuracy: 0.001°
Pitot Pressure (PP), psi		± 0.002 psi			± 0.010 psi		± 0.014 psi		< 10 psid	Druck ± 15 psid strain gage transducers	Analog to digital converter/digital data acquisition system	In-place application of multiple pressure levels measured with a pressure measuring device calibrated in the standards laboratory
Model Pressure (PW), psi		.00075 psi	>30	± 1.0		± (0.0015	psi + 1.0%)		0 ≤ P ≤ 0.15 psid	Druck ± 1 psid strain gage transducers	Analog to digital converter/digital data acquisition system	In-place application of multiple pressure levels measured with a pressure measuring device calibrated in the standards laboratory
		.002 psi	>30	± 0.1		± (0.004	psi + 0.1%)		0.15 ≤ P ≤ 1.5 psid			
		.002 psi	>30		± 0.003 psi	± 0.007	psi		< 2.5 psid	ESP[*] 2.5 psid strain gage transducer		
Model Temperature (TW), °F		± 1 °F	>30		± 2.2°F		± 4.2 °F		< 600 °F	Coaxial surface thermocouple gage	Digital data acquisition system/analog-to-digital converter	Thermocouple verification of NBS conformity/voltage substitution calibration
		± 1 °F	>30	± 0.375		± (0.375	% + 2 °F)		< 1600 °F			

[a]Reference: Abernethy, R.B. et al and Thompson, J. W. "Handbook Uncertainty in Gas Turbine Measurements." AEDC-TR-73-5, February 1973.

Note: [*] Bias assumed to be zero

32

TABLE 2. CONCLUDED

Parameter Designation	Steady-State Estimated Measurement[a]									Range	Type of Measuring Device	Type of Recording Device	Method of System Calibration
	Precision Index (S)			Bias (B)		Uncertainty ±(B + t95S)						
	Percent of Reading	Unit of Measurement	Degree of Freedom	Percent of Reading	Unit of Measurement	Percent of Reading	Unit of Measurement						
Probe Height Relative to Model Surface (ZP), in.		± 0.001 in.	>30		± 0.002 in.		± 0.004 psi			<9.0 in.	Potentiometer and Optical	Digital data acquisition system/analog-to-digital converter	Precision Micrometer
Survey Station (XSTA), in.		± 0.011 in.	>30		± 0.012 in.		± 0.034 in.			<26 in.	Potentiometer and Optical Graticule	Digital data acquisition System A/D Converter Optically Positioned Zero	Precision Micrometer
Heat Transfer (QDOT), Btu/ft²-sec		± 0.05 Btu/ft²-sec	>30	5		±(5% +	0.1 Btu/ft²-sec)			<1 Btu/ft²-sec	Coaxial surface thermocouple gage	Analog to digital converter/digital data acquisition system	Radiant heat source and secondary standard
ERMS, mv CURRENT, ma EBAR, mv	± 0.5 ± 0.5 ± 0.5			0 + 0 + 0 +		± 1 ± 1 ± 1				<1200 mv <5 ma <300 mv	Philco Ford Corp. Model #ADP-12/13 Hot-wire Anemometer System	Digital data acquisition system/analog-to-digital converter	Precision Digital Voltmeter

[a]Reference: Abernethy, R.B. et al and Thompson, J. W. "Handbook Uncertainty in Gas Turbine Measurements." AEDC-TR-73-5, February 1973.

Note: + Bias assumed to be zero

TABLE 3   TEST RUN SUMMARY

a. Hot-Wire Boundary-Layer Measurements at Location of Maximum Disturbance Energy - Run Summary

RE/FT x 10^{-6}	NOMINAL X STATION RUN NUMBERS																				
	10	11	12	13	14	15	16	17	18	19	20	21	22	23	24	25	26	27	28	29	30
1.0	65	64	63	62	61	60	59	58	57	56	55	54	53	52	51	50	49	48	47	46	45
																					66
1.5	84	83	82	81	80	79	78	77	76	75	74	73	72	71	70	69					

b. Boundary-Layer Profiles - Run Summary

RE/FT x 10^{-6}	NOMINAL X STATION RUN NUMBERS										
	10	20	22	24	26	28	30	32	34	36	37
1.0	99	98					97				96
1.5	95	94	93	92	91	90	89	88	87	86	

34

TABLE 3. CONCLUDED

c. Model Surface Data - Run Summary

RE/FT x 10^{-6}	Pressure and Temperature Data	Heat-Transfer Data
1.0	12, 19, 23, 24, 30, 44, 67, 100	1-4, 26, 27, 31-33
1.5	68, 85	5-9
2.0	--	10, 11

TABLE 4. ESTIMATED UNCERTAINTIES OF CALCULATED PARAMETERS

Parameter Designation	Precision Index (S)			Bias (B)		Uncertainty ± (B + t₉₅S)		RE/FT x 10⁻⁶ Nom.	MACH. Nominal
	Percent of Reading	Unit of Measurement	Degree of Freedom	Percent of Reading	Unit of Measurement	Percent of Reading	Unit of Measurement		
P, psi	1.23		<30	0.05		2.51		1.0	8.0
PT2, psia	0.85			0.05		1.75			
Q, psi	0.85			0.05		1.75			
T, °F	0.36			0.24		0.96			
V, ft/sec	0.04			0.12		0.20			
RHo, lbm/ft³	0.88			0.25		2.02			
MU, lbf-sec/ft²	0.36			0.24		0.96			
M	0.19 + +			0 +		0.38			
RE, per ft	0.53			0.37		1.42			
P, psi	0.82		<30	0.03		1.67		1.5	8.0
PT2, psia	0.57			0.03		1.17			
Q, psi	0.57			0.03		1.17			
T, °F	0.25			0.24		0.74			
V, ft/sec	0.04			0.12		0.20			
RHo, lbm/ft³	0.59			0.24		1.42			
MU, lbf-sec/ft²	0.25			0.24		0.74			
M	0.13 + +			0 +		0.26			
RE, per ft	0.36			0.37		1.09			

NOTE: +   Bias assumed to be zero

+ + Determined from test section repeatability and uniformity during tunnel calibration

36

HYPERSONIC BOUNDARY-LAYER STABILITY

RUN NUMBER   46   PAGE 1

CONFIG: HOLLOW CYLINDER (DIAM = 10 IN., RN = 0.0025 IN.)
XSTA = 30.00 IN.

DATA TYPE 9
HOT WIRE ANEMOMETER DATA

POINT	CURRENT (MAMP)	EBAR (MV)	ERMS (MV)	PT (PSIA)	TT (DEG R)	P (PSIA)	Q (PSIA)	T (DEG R)	RE (PER IN)	ZA (IN.)
1	1.998	228.22	226.39	2.249E+02	1.300E+03	2.407E-02	1.000E+00	9.818E+01	8.300E+04	3.075E-02
2	-0.001	-0.02	184.54	2.256E+02	1.300E+03	2.414E-02	1.044E+00	9.817E+01	8.305E+04	4.156E-01
3	1.994	258.84	290.56	2.256E+02	1.300E+03	2.414E-02	1.044E+00	9.817E+01	8.305E+04	4.156E-01

ALPHA = 0.02 DEG   XC   29.10 (IN)

MACH   7.93

PT = 224.90 PSIA   P = 2.407E-02 PSIA
TT = -1300.67 DEGR T = 9.818E+01 DEGR

Sample 1. Hot-Wire Anemometer Data

37

HYPERSONIC BOUNDARY-LAYER STABILITY

RUN NUMBER 97

CONFIG: HOLLOW CYLINDER (DIAM = 10 IN., RN = 0.0025 IN.)
XSTA =   30.00 IN.

DATA TYPE 4
FLOW FIELD SURVEYS

POINT	PT (PSIA)	TT (DEG R)	PT2 (PSIA)	P (PSIA)	ZP (IN)	PP (PSIA)	PWL (PSIA)	TWL (DEG R)	ZA (IN)	ERMS (MV RMS)

MEAN VALUES

PT = 224.2	PSIA	P = 0.0240	PSIA
TT = 1300.3	DEG R	PWL = 0.0245	PSIA
PT2 = 1.962E+05	PSIA	TWL = 548.0	DEG R
RE = 9.995E-08	PER FT	V = 3854.3	FT/SEC
MU = 7.905E-08	LBF-SEC/FT2	Q = 1.057	PSIA
RHO = 6.594E-04	LBM/FT3	T = 98.2	DEG R

PHI =   -0.01

M   =   7.93
ALPHA =   0.0 DEG R
DEW   = -57. DEG R

Sample 2. Flow-Field Survey Data

HYPERSONIC BOUNDARY-LAYER STABILITY

RUN NUMBER 97

CONFIG: HOLLOW CYLINDER (DIAM = 10 IN., RN = 0.0025 IN.)
XSTA = 30.00 IN.

DATA TYPE 4
FLOW FIELD SURVEYS

LOOP	ZP (IN)	PP/PPE	ML	ML/ME	TTL (DEG R)	TTL/TTE	TL (DEG R)	UL (FT/SEC)	UL/UE	LRE (PER IN)	LRET (PER IN)

MEAN VALUES

PT = 224.2 PSIA
TT = 1309.3 DEG R
P = 0.0240 PSIA
T = 98.2 DEG R

TWL/TTE = 0.4184
PML = 0.024
TWL = 548.0

M = 7.93 DEG
ALPHA = 0.0
PHI = -0.01

EDGE VALUES

PPE = 2.000E+00 PSIA
ME = 7.933E+00
TTE = 1.310E+03 DEG R
UE = 0.382E+04 FT/SEC

Sample 2. (Continued)

39

CONFIG: HOLLOW CYLINDER (DIAM = 10 IN., RN = 0.0025 IN.)
XSTA = 30.00 IN.

T/C	X (IN)	THETA (DEG)	TW (DEG R)	TW/TT
1	6.966	345	545.4	0.419
2	7.982	345	545.5	0.417
3	15.980	345	545.9	0.416
4	16.978	345	545.7	0.416
5	17.983	345	543.3	0.415
6	19.972	345	543.9	0.415
7	21.966	345	544.3	0.415
8	23.981	345	543.9	0.415
9	24.966	345	543.1	0.415
10	25.966	345	543.7	0.415
11	27.966	345	543.1	0.415
12	28.970	345	544.7	0.416
13	31.964	345	547.4	0.416
14	33.964	345	544.3	0.416
15	34.964	345	546.9	0.416
16	36.970	345	548.3	0.419
17	38.957	345	548.2	0.419
18	39.958	345	550.0	0.420
19	40.956	345	549.6	0.421
20	41.956	345	549.0	0.420
21	42.962	345	548.2	0.419

HYPERSONIC BOUNDARY-LAYER STABILITY

RUN NUMBER 97

DATA TYPE 4
MODEL SURFACE MEASUREMENTS

TAP	X (IN)	THETA (DEG)	PW (PSIA)	PW/P
1	37.721	15	0.0402	1.9229
2	38.215	15	0.0515	2.1447
3	40.712	15	0.0430	1.8276
4	42.224	15	0.0310	1.3208
5	45.700	15	0.0201	1.2122
6	46.216	15	0.0309	1.2407
7	46.720	15	0.0283	1.1811
8	47.253	15	0.0275	1.2188
9	8.071	90	0.0292	1.1599
10	11.073	90	0.0273	1.1379
11	19.060	90	0.0254	1.1067
12	25.071	90	0.0275	1.0742
13	29.073	90		1.1442
14	7.070	100	0.0280	1.0444
15	8.071	100	0.0298	2.0020
16	11.904	100	0.0264	1.1840
17	10.071	100	0.0266	1.1681
18	25.074	100	0.0301	1.0561
19	7.070	270	0.0247	1.1641
20	9.067	270	0.0285	1.1800
21	11.066	270	0.0302	1.2580
22	19.070	270	0.0208	1.2003
23	25.071	270	0.0222	1.1742
24	29.073	270	0.0235	1.0610

ALPHA = 0.0 DEG
PHI = 0.0 DEG

XC = 30.000

PT = 224.2 PSIA
TT = 1369.3 DEG R
M = 7.933
RE = 0.999E+06 /FT

TDRK = 554.7 DEG R
P = 0.0240 PSIA
T = 98.2344 DEG R

Sample 2. (Continued)

```
                                                                                          DATE COMPUTED  25-OCT-89
                                                                                          DATE RECORDED  14-AUG-89
                                                                                          TIME RECORDED   9: 2: 17
                                                                                          TIME COMPUTED  07:24:55
HYPERSONIC BOUNDARY-LAYER STABILITY                                                       PROJECT NUMBER C010VB

 RUN NUMBER   97                                     CONFIG: HOLLOW CYLINDER (DIAM = 10 IN., RN = 0.0025 IN.)
                                                     XSTA =   30.00  IN.

    DATA TYPE 4
    INTEGRAL EVALUATION

  LOOP     ZP/DEL     PP/PPD      ML/MD     TTL/TTD     TL/TD    RHOL/RHOD    UL/UD    MUTL/MUTD  LRE/LRED  DITTL/DITTD LRET/LRETD

    1    1.205E-01  1.841E-02  7.771E-02  4.833E-01  5.278E+00  1.895E-01  1.785E-01  4.543E+00  7.447E-03  1.275E-01 5.465E-02
    2    1.461E-01  2.004E-02  9.867E-02  5.173E-01  5.340E+00  1.873E-01  2.280E-01  4.584E+00  9.315E-03  1.674E-01 6.663E-02
    3    1.905E-01  1.982E-02  8.363E-02  4.999E-01  5.298E+00  1.888E-01  1.925E-01  4.557E+00  7.974E-03  1.385E-01 5.813E-02
    4    2.041E-01  2.145E-02  1.030E-01  5.224E-01  5.349E+00  1.870E-01  2.382E-01  4.590E+00  9.705E-03  1.759E-01 6.901E-02
    5    2.287E-01  2.004E-02  9.867E-02  5.173E-01  5.340E+00  1.873E-01  2.280E-01  4.584E+00  9.315E-03  1.674E-01 6.663E-02
    6    2.757E-01  2.206E-02  1.071E-01  5.273E-01  5.356E+00  1.867E-01  2.479E-01  4.594E+00  1.007E-02  1.841E-01 7.121E-02
    7    3.013E-01  2.509E-02  1.246E-01  5.488E-01  5.373E+00  1.861E-01  2.888E-01  4.605E+00  1.167E-02  2.201E-01 8.037E-02
    8    3.337E-01  3.177E-02  1.529E-01  5.857E-01  5.358E+00  1.867E-01  3.539E-01  4.595E+00  1.438E-02  2.819E-01 9.432E-02
    9    3.524E-01  3.603E-02  1.873E-01  6.044E-01  5.324E+00  1.878E-01  3.860E-01  4.574E+00  1.585E-02  3.134E-01 1.013E-01
   10    3.787E-01  4.332E-02  1.989E-01  6.318E-01  5.242E+00  1.908E-01  4.324E-01  4.522E+00  1.824E-02  3.600E-01 1.117E-01
   11    4.138E-01  5.406E-02  2.181E-01  6.681E-01  5.085E+00  1.967E-01  4.819E-01  4.410E+00  2.109E-02  4.213E-01 1.261E-01
   12    4.411E-01  6.883E-02  2.487E-01  7.047E-01  4.880E+00  2.049E-01  5.404E-01  4.284E+00  2.628E-02  4.830E-01 1.415E-01
   13    4.735E-01  8.402E-02  2.780E-01  7.385E-01  4.661E+00  2.146E-01  6.001E-01  4.136E+00  3.113E-02  5.418E-01 1.560E-01
   14    4.940E-01  9.982E-02  3.054E-01  7.691E-01  4.445E+00  2.250E-01  6.430E-01  3.987E+00  3.633E-02  5.948E-01 1.717E-01
   15    5.179E-01  1.205E-01  3.378E-01  8.023E-01  4.177E+00  2.394E-01  6.904E-01  3.798E+00  4.352E-02  6.521E-01 1.905E-01
   16    5.400E-01  1.417E-01  3.682E-01  8.301E-01  3.922E+00  2.550E-01  7.292E-01  3.612E+00  5.148E-02  7.005E-01 2.095E-01
   17    5.673E-01  1.697E-01  4.047E-01  8.604E-01  3.625E+00  2.759E-01  7.705E-01  3.388E+00  6.274E-02  7.533E-01 2.340E-01
   18    5.946E-01  1.976E-01  4.381E-01  8.842E-01  3.361E+00  2.975E-01  8.032E-01  3.182E+00  7.510E-02  7.950E-01 2.585E-01
   19    6.202E-01  2.268E-01  4.784E-01  9.038E-01  3.118E+00  3.207E-01  8.307E-01  2.986E+00  8.922E-02  8.294E-01 2.842E-01
   20    6.543E-01  2.651E-01  5.098E-01  9.241E-01  2.843E+00  3.517E-01  8.596E-01  2.757E+00  1.097E-01  8.654E-01 3.179E-01
   21    6.816E-01  3.064E-01  5.491E-01  9.417E-01  2.594E+00  3.854E-01  8.844E-01  2.542E+00  1.341E-01  8.964E-01 3.541E-01
   22    7.174E-01  3.677E-01  6.027E-01  9.611E-01  2.292E+00  4.363E-01  9.126E-01  2.270E+00  1.754E-01  9.300E-01 4.083E-01
   23    7.446E-01  4.285E-01  6.515E-01  9.742E-01  2.050E+00  4.877E-01  9.320E-01  2.044E+00  2.226E-01  9.541E-01 4.626E-01
   24    7.736E-01  4.886E-01  6.965E-01  9.825E-01  1.852E+00  5.398E-01  9.479E-01  1.852E+00  2.763E-01  9.688E-01 5.175E-01
   25    8.060E-01  5.567E-01  7.440E-01  9.892E-01  1.668E+00  5.994E-01  9.611E-01  1.668E+00  3.453E-01  9.807E-01 5.809E-01
   26    8.163E-01  5.889E-01  7.655E-01  9.917E-01  1.583E+00  6.277E-01  9.663E-01  1.583E+00  3.807E-01  9.852E-01 6.097E-01
   27    8.555E-01  6.867E-01  8.274E-01  9.972E-01  1.400E+00  7.143E-01  9.789E-01  1.400E+00  4.995E-01  9.949E-01 7.005E-01
   28    8.896E-01  7.675E-01  8.761E-01  9.995E-01  1.271E+00  7.869E-01  9.866E-01  1.271E+00  6.108E-01  9.992E-01 7.765E-01
   29    9.237E-01  8.507E-01  9.218E-01  1.000E+00  1.159E+00  8.627E-01  9.925E-01  1.159E+00  7.386E-01  1.001E+00 8.560E-01
   30    9.322E-01  8.756E-01  9.353E-01  1.000E+00  1.129E+00  8.856E-01  9.930E-01  1.129E+00  7.795E-01  1.000E+00 8.800E-01
   31    9.646E-01  9.394E-01  9.690E-01  1.000E+00  1.059E+00  9.439E-01  9.974E-01  1.059E+00  8.887E-01  1.001E+00 9.412E-01
   32    9.970E-01  9.953E-01  9.976E-01  1.000E+00  1.004E+00  9.957E-01  9.998E-01  1.004E+00  9.912E-01  1.000E+00 9.954E-01
   33    1.009E+00  1.014E+00  1.007E+00  9.998E-01  9.875E-01  1.013E+00  1.000E+00  9.875E-01  1.026E+00  9.997E-01 1.013E+00
   34    1.057E+00  1.076E+00  1.037E+00  9.986E-01  9.339E-01  1.071E+00  1.002E+00  9.339E-01  1.149E+00  9.976E-01 1.074E+00
   35    1.074E+00  1.093E+00  1.046E+00  9.982E-01  9.201E-01  1.087E+00  1.003E+00  9.201E-01  1.185E+00  9.969E-01 1.091E+00
   36    1.106E+00  1.118E+00  1.058E+00  9.976E-01  9.000E-01  1.111E+00  1.003E+00  9.000E-01  1.239E+00  9.957E-01 1.117E+00
   37    1.123E+00  1.127E+00  1.062E+00  9.973E-01  8.935E-01  1.119E+00  1.004E+00  8.935E-01  1.257E+00  9.952E-01 1.125E+00
   38    1.191E+00  1.159E+00  1.077E+00  9.963E-01  8.696E-01  1.150E+00  1.004E+00  8.696E-01  1.328E+00  9.934E-01 1.158E+00
   39    1.229E+00  1.168E+00  1.081E+00  9.960E-01  8.630E-01  1.159E+00  1.004E+00  8.630E-01  1.349E+00  9.929E-01 1.167E+00
   40    1.301E+00  1.179E+00  1.087E+00  9.956E-01  8.548E-01  1.170E+00  1.005E+00  8.548E-01  1.375E+00  9.922E-01 1.179E+00
   41    1.353E+00  1.184E+00  1.089E+00  9.955E-01  8.518E-01  1.174E+00  1.005E+00  8.518E-01  1.385E+00  9.919E-01 1.183E+00
   42    1.418E+00  1.193E+00  1.093E+00  9.951E-01  8.450E-01  1.183E+00  1.005E+00  8.450E-01  1.407E+00  9.913E-01 1.193E+00
   43    1.473E+00  1.198E+00  1.095E+00  9.950E-01  8.421E-01  1.188E+00  1.005E+00  8.421E-01  1.417E+00  9.910E-01 1.197E+00
   44    1.517E+00  1.203E+00  1.097E+00  9.948E-01  8.388E-01  1.192E+00  1.005E+00  8.388E-01  1.428E+00  9.907E-01 1.202E+00
   45    1.567E+00  1.205E+00  1.098E+00  9.947E-01  8.371E-01  1.195E+00  1.005E+00  8.371E-01  1.434E+00  9.905E-01 1.205E+00
   46    1.621E+00  1.209E+00  1.100E+00  9.945E-01  8.347E-01  1.198E+00  1.005E+00  8.347E-01  1.443E+00  9.903E-01 1.208E+00
   47    1.688E+00  1.213E+00  1.102E+00  9.944E-01  8.318E-01  1.202E+00  1.005E+00  8.318E-01  1.453E+00  9.900E-01 1.213E+00

                                                              VALUES AT DELTA

                                   DEL   = 4.303E-01 IN       PPD = 1.649E+00 PSIA           RHOD = 5.716E-04 LBM/FT3
      M =    7.93                  DEL*  = 3.088E-01 IN       MD  = 7.1987E+00              RHOUD = 2.171E+00 LBM/SEC-FT2
  ALPHA =    0.0   DEG             DEL** = 1.394E-02 IN       TD  = 1.159E+02 DEG R          MUTD = 9.326E-08 LBF-SEC/FT2
                                                              TTO = 1.317E+03 DEG R         DITTD = 1.913E+02 BTU/LBM
                                   LRED = 6.031E+04 PER IN    UD  = 3.709E+03 FT/SEC        LRETD = 7.857E+03 PER IN
      PHI  =  -0.01
```

Sample 2. (Concluded)

CONFIG: HOLLOW CYLINDER (DIAM = 10 IN., RN = 0.0025 IN.)
XSTA = 0.00 IN.

T/C	X (IN)	THETA (DEG)	TW (DEG R)	TW/TT
1	6.900	345	543.6	0.418
2	7.943	345	543.0	0.417
3	15.989	345	542.7	0.417
4	16.970	345	543.7	0.416
5	17.963	345	544.9	0.416
6	19.972	345	544.8	0.416
7	21.964	345	544.0	0.413
8	22.964	345	541.8	0.416
9	23.961	345	544.0	0.416
10	24.966	345	544.2	0.416
11	25.975	345	544.1	0.416
12	27.966	345	542.1	0.417
13	28.964	345	544.1	0.417
14	28.970	345	544.1	0.416
15	31.966	345	543.3	0.416
16	32.966	345	544.7	0.416
17	33.964	345	544.1	0.416
18	34.954	345	544.0	0.416
19	35.964	345	544.1	0.416
20	36.970	345	544.6	0.416
21	37.969	345	545.4	0.416
22	38.957	345	545.2	0.414
23	39.958	345	542.0	0.416
24	40.958	345	547.3	0.416
25	41.958	345		
26	42.962	345		

HYPERSONIC BOUNDARY-LAYER STABILITY

RUN NUMBER   85   PAGE 1

DATA TYPE 2
MODEL SURFACE MEASUREMENTS

TAP	X (IN)	THETA (DEG)	PW (PSIA)	PW/P
1	3.721	15	0.0344	0.9865
2	38.215	15	0.0370	1.0370
3	40.712	15	0.0378	1.0613
4	42.224	15	0.0348	0.9773
5	43.760	15	0.0398	1.0532
6	45.216	15	0.0377	1.0041
7	46.728	15	0.0377	1.0579
8	47.228	90	0.0366	1.0273
9	47.973	90	0.0391	1.0965
10	8.971	90	0.0355	0.9906
11	11.973	90	0.0377	1.0594
12	19.969	90	0.0366	1.0279
13	25.971	90	0.0363	1.0184
14	28.973	90	0.0367	1.0306
15	7.970	180	0.0400	1.1233
16	8.971	180	0.0404	
17	11.968	180	0.0328	1.1355
18	19.968	180	0.0377	1.2207
19	25.974	180	0.0357	1.0570
20	28.969	180	0.0382	1.0024
21	7.970	270	0.0387	1.0730
22	9.967	270	0.0400	1.1134
23	11.966	270	0.0409	1.1498
24	19.970	270	0.0336	0.9436
25	25.971	270	0.0373	0.0473
26	29.973	270	0.0365	1.0242

ALPHA = 0.0 DEG
PHI = 0.0 DEG

XC = 23.418

PT = 336.6 PSIA
TT = 1310.7 DEG R
M = 7.050
RE = 0.150E+07 /FT

TDRK = 550.7 DEG R
P = 0.0358 PSIA
T = 97.8101 DEG R

Sample 3. Model Surface Measurements

42

DATE COMPUTED: 4-AUG-89
TIME COMPUTED: 02:46:07
DATE RECORDED: 4-AUG-89
TIME RECORDED: 2:45:28
000000129

PAGE 1

HYPERSONIC B L STABILITY VKF
PROJECT NUMBER: CI24V8

RUN NUMBER 5

DATA TYPE: SURFACE HEAT TRANSFER

HOLLOW CYLINDER (DIAM=10.0 IN., RN=0.002 IN.)

GAGE NO	X IN.	THETA DEG	QDOT BTU/FT2-SEC	TW DEG.R	HT(TT) BTU/FT2-SEC-R	ST(TT)
1	7.00	345.	0.266	541.35	3.457E-04	3.600E-04
2	7.98	345.	0.254	540.99	3.299E-04	3.492E-04
3	15.98	345.	0.189	540.89	2.459E-04	2.603E-04
4	16.98	345.	0.180	541.18	2.342E-04	2.470E-04
5	17.98	345.	0.158	541.13	1.957E-04	2.071E-04
6	19.97	345.	0.173	540.62	2.240E-04	2.300E-04
7	21.97	345.	0.182	540.83	2.369E-04	2.500E-04
8	22.99	345.	0.175	540.57	2.282E-04	2.415E-04
9	23.98	345.	0.156	540.09	2.035E-04	2.152E-04
10	24.97	345.	0.177	540.57	2.307E-04	2.531E-04
11	25.97	345.	0.190	541.04	2.477E-04	2.618E-04
12	26.98	345.	0.211	541.30	2.755E-04	2.910E-04
13	27.97	345.	0.211	541.00	2.790E-04	2.911E-04
14	28.97	345.				
16	31.97	345.	0.243	542.19	3.173E-04	3.358E-04
17	32.97	345.	0.282	541.42	3.673E-04	3.887E-04
18	33.96	345.	0.317	541.30	4.054E-04	4.282E-04
19	34.95	345.	0.327	541.29	4.252E-04	4.501E-04
20	35.96	345.	0.362	541.72	4.715E-04	4.991E-04
21	36.97	345.	0.380	541.58	4.954E-04	5.243E-04
22	37.97	345.	0.413	541.58	5.382E-04	5.697E-04
23	38.96	345.	0.438	542.00	5.706E-04	6.033E-04
24	39.96	345.	0.438	542.12	5.784E-04	6.038E-04
25	40.96	345.	0.472	542.17	6.151E-04	6.511E-04
26	41.96	345.	0.528	542.13	6.773E-04	7.169E-04
27	42.96	345.	0.526	542.53	6.862E-04	7.263E-04

PHI = -0.02 DEG
M = 7.96
ALPHA = -0.03 DEG
DEW = -757.00 DEG.F

PT = 349.11 PSIA
TT = 1309.67 DEG.R
P = 0.04 PSIA
RE = 1.504E+06 PER FT
MU = 7.857E-08 LBF-SEC/FT2

V = 3856.98 FT/SEC
Q = 1.583 PSIA
T = 97.64 DEG.R
PT2 = 2.94 PSIA
RHO = 9.857E-04 LBM/FT3

RUN NUMBER 5

Sample 4. Model Surface Heat-Transfer Data